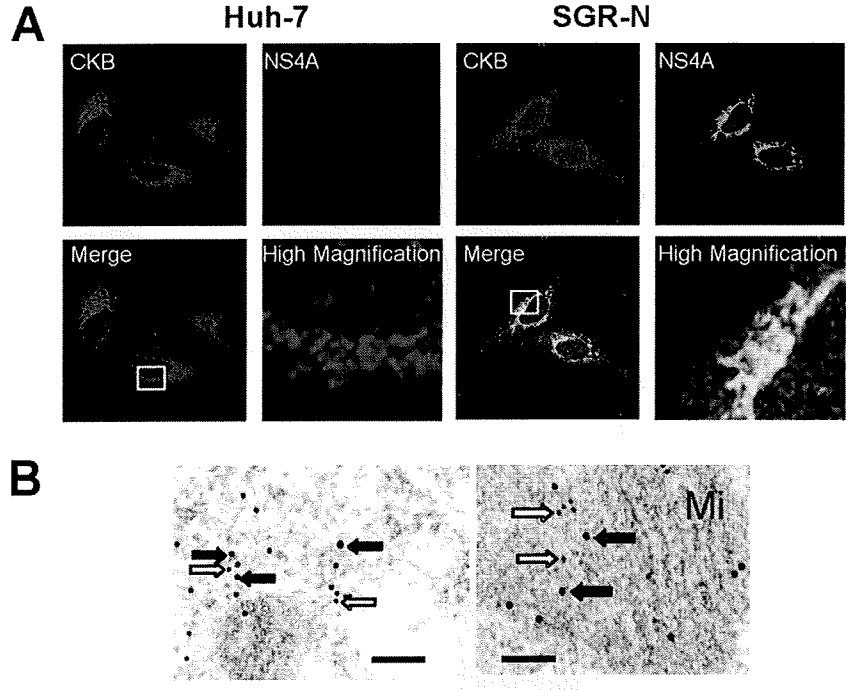

FIG. 4. Colocalization of CKB with HCV NS4A. (A) Indirect immunofluorescence analysis. The primary antibodies used were anti-CKB goat PAb (red) and anti-NS4A MAb (green). Merged images of red and green signals are shown. High-magnification panels are enlarged images of white squares in the merge panels. (B) Immunoelectron microscopic localization of CKB and NS4A. SGR-N cells were double-immunolabeled for CKB (12-nm gold particles; white arrows) and for NS4A (18-nm gold particle; gray arrows). Mi, mitochondria. Bars, 200 nm.

CKB colocalized with NS4A in the cytoplasmic electron-dense regions, presumably derived from altered or folded membrane structures (Fig. 4B, left panel) and mitochondria (Fig. 4B, right panel).

CKB enhances functional HCV replicase and NS3-4A helicase. NS4A is known to mediate membrane association of the NS3-4A complex and to function as a cofactor in NS3 enzyme activity. To understand the mechanism(s) underlying positive regulation of HCV RNA replication through CKB via its interaction with NS4A, we first investigated whether CKB modulates NS3-4A helicase activity. NS3-4A helicase is a member of the superfamily-2 DexH/D-box helicase, which unwinds RNA-RNA substrates in a 3′-to-5′ direction. During RNA replication, the NS3-4A helicase is believed to translocate along the nucleic acid substrate by changing its protein conformation, utilizing the energy of ATP hydrolysis (9). We then tested the effect of CKB on RNA- or DNA-unwinding activity using purified recombinant full-length NS3 and NS3-4A complex (12). As shown in Fig. 5A (left middle panel), both NS3 and NS3-4A helicase activity unwound dsRNA substrate most efficiently when CKB, ATP, and pCr were added to the reaction mixture. The enhancing effect of CKB was observed in the presence of pCr but not in the absence of it, suggesting that catalytic activity of CKB is important for its effect on the HCV helicase activity. Similar results were obtained from the DNA helicase assay using dsDNA substrate (Fig. 5B). To address the specificity of the stimulation by the CKB/pCr system, effects of PK and pPy, which are also involved in the ATP generation, were determined (Fig. 5A, right panels). Exogenous PK and pPy at the same concentrations as those of CKB and pCr used in the study exhibited no effect on the HCV helicase activity.

The effect of CKB on NS3-4A serine protease activity, which is considered to be ATP-independent, was also assessed in an in vitro protease assay using the purified viral proteins as mentioned above (Fig. 5C). As expected, NS3-4A complex exhibited significantly higher activity than NS3 alone; however, CKB did not affect the protease activities of NS3 or NS3-4A.

Finally, we investigated loss and gain of function of CKB in HCV replicase activity, which requires high-energy phosphate, in the context of semi-intact replicon cells. Miyanari et al. (33) reported that the function of the active HCV RC can be monitored in permeabilized replicon cells treated with digitonin. Thus, permeabilized replicon cells in the presence or absence of exogenous CKB were incubated with [α-^{32}P]UTP to detect newly synthesized RNA. As indicated in Fig. 5D, an ~8-kb band corresponding to HCV subgenomic RNA was most abundant in cells in the presence of exogenous CKB, ATP and pCr. The enhancing effect of CKB was observed in the presence but not in the absence of pCr, suggesting that catalytic activity of CKB is important for its effect on the replicase activity. As for the RNA helicase assay, exogenous PK and pPy did not enhance the replicase activity (data not shown). HCV replicase activity in permeabilized cells to which we had introduced siCKB-2 was diminished compared to that in siRNA control-treated cells. Interestingly, the replicase activity in the CKB-depleted cells was recovered by the addition of CKB. Thus, our findings suggest that CKB functions as a key regulator of HCV genome replication by controlling energy-dependent viral enzyme activities.

Downloaded from jvi.asm.org at National Institute of Infectious Diseases on March 15, 2010

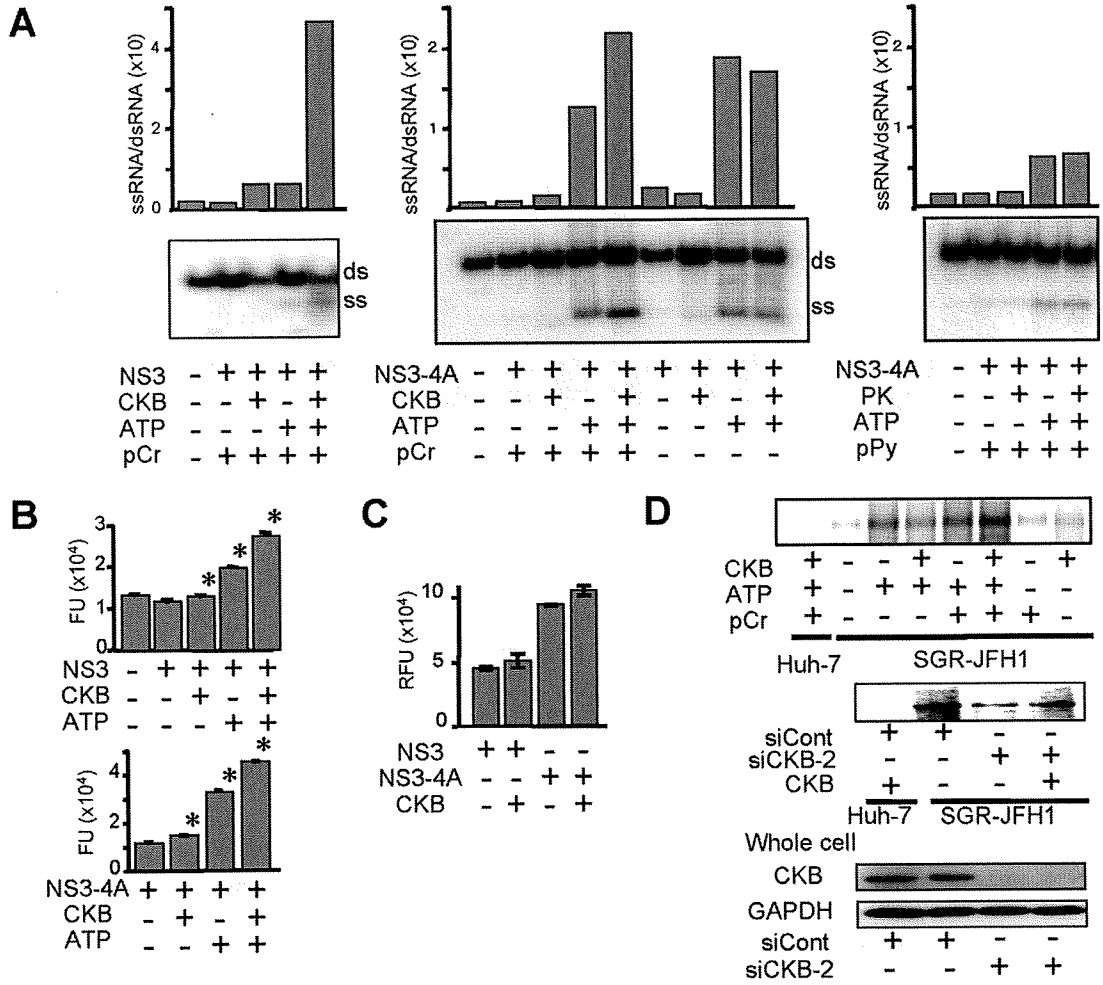

FIG. 5. CKB enhances NS3-4A helicase and HCV replicase activities. (A) In vitro RNA helicase activity of NS3-4A or NS3 was determined by detecting unwound single-strand RNA (ss) derived from the partially dsRNA substrate (ds). Band intensities corresponding to unwound products and those to dsRNA substrates were determined by ImageQuant 5.2 (Molecular Dynamics), and the ssRNA/dsRNA ratios were calculated. The results are representative of three similar experiments. (B) In vitro DNA helicase activity of NS3-4A or NS3 was analyzed by using a commercially available kit. The data represent averages and standard deviations ($n = 3$). *, $P < 0.05$ against the value without supplementation of CKB and ATP. (C) The in vitro HCV protease activity of NS3-4A or NS3 in the presence or absence of CKB was analyzed. Error bars represent standard deviations ($n = 3$). (D) Replicase activity in permeabilized replicon cells. The upper panel shows the activity for synthesis of HCV subgenomic RNA in the digitonin-permeabilized SGR-JFH1 cells with or without supplementation of CKB was measured. The middle panel shows results for SGR-JFH1 or Huh-7 cells that were transfected with siCKB-2 or siCont and permeabilized at 72 h posttransfection. The permeabilized cells with or without supplementation of CKB were subjected to the replicase assay. The lower panel shows the immunoblotting results for whole-cell lysates of siRNA-transfected cells.

DISCUSSION

Viral replication requires energy and macromolecule synthesis, and host cells provide the viruses with metabolic resources necessary for their efficient replication. Thus, it is highly likely that interaction of viruses with host cell metabolic pathways, including energy-generating systems, contributes to the virus growth cycle. In the regulation of HCV genome replication, the functions of the viral NS proteins that comprise the RC might be regulated by association in individual host cell factors. For example, hVAP-A and -B function as cofactors of modulating RC formation via interacting with NS5A and NS5B (13, 18). Cyclophilin B is involved in stimulating viral RNA binding activity via interacting with NS5B (49). FKBP8 (39) and hB-ind1 (45) play an important role in recruiting Hsp90 to RC via interacting with NS5A. However, the association of viral protein(s) with the cellular energy-generating system to directly regulate the activity of the RC has not been well understood.

In the present study, the accumulation of CKB, an ATP-generating enzyme, in the HCV RC-rich membrane fraction of viral replicating cells and its importance in replication of the HCV genome and production of infectious virions have been demonstrated. Enzymatic analyses with semi-intact replicon cells and purified NS3-4A protein revealed that CKB enhances the functional replicase and helicase of HCV. Its enhancing effect was observed in the presence of pCr but not in its absence, suggesting that the catalytic activity of CKB is important for enhancing the replicase and

Downloaded from jvi.asm.org at National Institute of Infectious Diseases on March 15, 2010

helicase activities. Moreover, we clearly detected a CKB-NS4A complex using anti-tag antibodies in cotransfection experiments, but the endogenous complex could not be immunoprecipitated from cells expressing only endogenous levels of CKB, probably because of the inefficiency of the available antibodies. Further, a deletion of the NS4A-interacting region within an inactive mutant of CKB (CKB-C283S) resulted in the loss of its dominant-negative effect on HCV replication.

Creatine kinase, an evolutionarily conserved enzyme, is known to be critical for the maintenance and regulation of cellular energy stores in tissues with high and rapidly changing energy demands (48). In mammals, three cytosolic and two mitochondrial isoforms of CK, which share certain conserved regions, are expressed (35). The brain-type CK, CKB, plays a major role in cellular energy metabolism of nonmuscle cells, reversibly catalyzing the ATP-dependent phosphorylation of creatine and, hence, providing an ATP buffering system in subcellular compartments of high and fluctuating energy demand (21, 29). CKB is overexpressed in a wide range of tumor tissues and tumor cell lines, including hepatocellular carcinoma (32), and is used as a prognostic marker of cancer.

Although CK and creatine phosphate have been supplemented to in vitro replicase assays of some RNA viruses (15, 33), understanding of CKB function in the virus life cycle has been limited. One study indicated that the CK substrate analog, Ccr, exhibits antiviral activity against several herpesviruses but not influenza viruses or vesicular stomatitis virus (26). We have demonstrated here that HCV genome replication is downregulated by either treatment with Ccr, siRNA-mediated knockdown of CKB, or the exogenous expression of CKB-C283S. Coimmunoprecipitation experiments revealed that the essential domain within NS4A for the interaction with CKB is the NS4A central domain, aa 21 to 39, which is also responsible for NS3-4A complex formation. However, the NS3-4A interaction was not impaired by overexpression of CKB, and CKB was found to be able to form a complex with NS3-4A (Fig. 3H). Since CKB does not directly interact with NS3 (Fig. 3A), it is likely that NS3-4A-CKB association occurs through two interactions of NS3-4A and NS4A-CKB. We examined whether the formation of the ternary complex affects HCV enzymatic activities, possibly through conformational changes in the viral proteins, and found that CKB has no influence on NS3-4A protease activity (Fig. 5C). With regard to helicase activity, the effect of CKB on RNA unwinding activity by NS3-4A was similar to the effect of NS3 alone in the presence of ATP (Fig. 5A). It is conceivable that interaction with CKB causes no or little global change in the NS3-4A conformation and does not affect the viral helicase and protease activities.

In general, translation initiation in eukaryotes includes an ATP-dependent process such as unwinding the secondary structure in the 5′-untranslated region to permit assembly of 48S ribosomal complexes. It was reported, however, that 48S complex formation on the HCV internal ribosome entry site (IRES) has no requirement for ATP hydrolysis (25). In fact, we found that Huh-7 cells with or without gene silencing of CKB exhibited the same level of HCV IRES activity by transfection with IRES-reporter constructs (data not shown).

Collectively, we conclude that CKB is targeted to the HCV RC through its interaction with NS4A and functions as a positive regulator for the viral replicase by providing ATP. It is likely that the catalytic activity of CKB that associates with the viral RC is important for enhancing the RNA replication. The role of CKB-NS4A interaction in the enhancing effect seems to be limited. Although either knocking down CKB, expression of the dominant-negative mutant of CKB, or Ccr treatment resulted in the reduction of HCV replication (Fig. 2A to C), the total cellular ATP levels were not changed under these conditions (Fig. 2D). This suggests that CKB contributes to enhancing HCV replication through controlling the ATP level in the particular RC compartment. A tight coupling of a fast ATP regeneration and delivery system to the viral RC is advantageous for achieving efficient replication of the viral genome. To our knowledge, the findings presented here provide the first experimental evidence of the involvement of viral protein in recruiting an ATP generating/buffering system to the subcellular compartment for viral genome replication, a site with high-energy turnover. Given that the levels of HCV RNA were not dramatically diminished by the knocking down, dominant-negative mutant or Ccr, CKB may not be absolutely critical for the viral replication. One would argue that energy required for HCV genome replication can be partly complemented from the intracellular ATP pool.

Although there are several isoforms of CK as described above, the most abundant CK species expressed in Huh-7 cells in the present study was CKB, and no other isoenzymes, including mitochondrial CK, were detected by an isoform analysis based on the overlay gel technique (32; data not shown). Thus, the CKB isoenzyme appears to be a key molecule in the energy metabolism of HCV replicating cells. To identify potential HCV RC components, we used a comparative proteome analysis of the DRM fraction in cells harboring HCV subgenomic replicon and the DRM fractions in parental cells and then identified proteins that were more abundant in the fraction of HCV replicating cells. In agreement with similar previously reported approaches using the DRM or lipid raft fraction (30, 53), the functional categories of identified proteins included protein folding or assembly, cell metabolism and biosynthesis, cellular processes, and cytoskeleton organization (Table 1). Interestingly, Mannova et al. found that CKB was upregulated in the fraction of Huh-7 cells carrying the genotype 1b Con1 isolate-derived HCV replicon, as determined using stable isotope labeling by amino acids combined with one-dimensional electrophoresis (30). However, the effect of CKB on regulation of the HCV life cycle was not examined in that study.

In conclusion, CKB interacts with HCV NS4A and is important for efficient replication of the viral genome. Recruitment of CKB to the HCV replication machinery through its interaction with NS4A may have important implications for the maintenance or enhancement of the functional replicase activity in the RC compartment, where high-energy phosphoryl groups are required. A strategy for specific interception of energy supply at the subcellular site of HCV genome replication by disruption of the NS4A-CKB interface may lead to development of a new type of antiviral agent.

ACKNOWLEDGMENTS

We thank Francis V. Chisari (The Scripps Research Institute) for providing Huh-7.5.1 cells; Raffaele De Francesco (Istituto di Ricerche

Downloaded from jvi.asm.org at National Institute of Infectious Diseases on March 15, 2010

di Biologia Molecolare, P. Angeletti) for providing purified recombinant NS3 and NS3-4A proteins; Oriental Yeast Co., Ltd., for providing human CKB cDNA; Minoru Fukuda (Laboratory for Electron Microscopy, Kyorin University School of Medicine) for electron microscopy; S. Yoshizaki, T. Shimoji, M. Kaga, M. Sasaki, and T. Date for technical assistance; and T. Mizoguchi for secretarial work.

This study was supported by a grant-in-aid for Scientific Research from the Japan Society for the Promotion of Science, from the Ministry of Health, Labor, and Welfare of Japan and from the Ministry of Education, Culture, Sports, Science, and Technology and by Research on Health Sciences focusing on Drug Innovation from the Japan Health Sciences Foundation, Japan, and by the Program for Promotion of Fundamental Studies in Health Sciences of the National Institute of Biomedical Innovation of Japan.

REFERENCES

1. **Aizaki, H., Y. Aoki, T. Harada, K. Ishii, T. Suzuki, S. Nagamori, G. Toda, Y. Matsuura, and T. Miyamura.** 1998. Full-length complementary DNA of hepatitis C virus genome from an infectious blood sample. Hepatology **27:** 621–627.
2. **Aizaki, H., K. J. Lee, V. M. Sung, H. Ishiko, and M. M. Lai.** 2004. Characterization of the hepatitis C virus RNA replication complex associated with lipid rafts. Virology **324:**450–461.
3. **Aizaki, H., K. Morikawa, M. Fukasawa, H. Hara, Y. Inoue, H. Tani, K. Saito, M. Nishijima, K. Hanada, Y. Matsuura, M. M. Lai, T. Miyamura, T. Wakita, and T. Suzuki.** 2008. Critical role of virion-associated cholesterol and sphingolipid in hepatitis C virus infection. J. Virol. **82:**5715–5724.
4. **Alter, H. J., and L. B. Seeff.** 2000. Recovery, persistence, and sequelae in hepatitis C virus infection: a perspective on long-term outcome. Semin. Liver Dis. **20:**17–35.
5. **Aoyagi, K., C. Ohue, K. Iida, T. Kimura, E. Tanaka, K. Kiyosawa, and S. Yagi.** 1999. Development of a simple and highly sensitive enzyme immunoassay for hepatitis C virus core antigen. J. Clin. Microbiol. **37:**1802–1808.
6. **Appel, N., T. Schaller, F. Penin, and R. Bartenschlager.** 2006. From structure to function: new insights into hepatitis C virus RNA replication. J. Biol. Chem. **281:**9833–9836.
7. **Bartenschlager, R., and V. Lohmann.** 2001. Novel cell culture systems for the hepatitis C virus. Antivir. Res. **52:**1–17.
8. **Brass, V., J. M. Berke, R. Montserret, H. E. Blum, F. Penin, and D. Moradpour.** 2008. Structural determinants for membrane association and dynamic organization of the hepatitis C virus NS3-4A complex. Proc. Natl. Acad. Sci. USA.
9. **Dumont, S., W. Cheng, V. Serebrov, R. K. Beran, I. Tinoco, Jr., A. M. Pyle, and C. Bustamante.** 2006. RNA translocation and unwinding mechanism of HCV NS3 helicase and its coordination by ATP. Nature **439:**105–108.
10. **Failla, C., L. Tomei, and R. De Francesco.** 1994. Both NS3 and NS4A are required for proteolytic processing of hepatitis C virus nonstructural proteins. J. Virol. **68:**3753–3760.
11. **Gallinari, P., D. Brennan, C. Nardi, M. Brunetti, L. Tomei, C. Steinkuhler, and R. De Francesco.** 1998. Multiple enzymatic activities associated with recombinant NS3 protein of hepatitis C virus. J. Virol. **72:**6758–6769.
12. **Gallinari, P., C. Paolini, D. Brennan, C. Nardi, C. Steinkuhler, and R. De Francesco.** 1999. Modulation of hepatitis C virus NS3 protease and helicase activities through the interaction with NS4A. Biochemistry **38:**5620–5632.
13. **Gao, L., H. Aizaki, J. W. He, and M. M. Lai.** 2004. Interactions between viral nonstructural proteins and host protein hVAP-33 mediate the formation of hepatitis C virus RNA replication complex on lipid raft. J. Virol. **78:**3480–3488.
14. **Gosert, R., D. Egger, V. Lohmann, R. Bartenschlager, H. E. Blum, K. Bienz, and D. Moradpour.** 2003. Identification of the hepatitis C virus RNA replication complex in Huh-7 cells harboring subgenomic replicons. J. Virol. **77:**5487–5492.
15. **Green, K. Y., A. Mory, M. H. Fogg, A. Weisberg, G. Belliot, M. Wagner, T. Mitra, E. Ehrenfeld, C. E. Cameron, and S. V. Sosnovtsev.** 2002. Isolation of enzymatically active replication complexes from feline calicivirus-infected cells. J. Virol. **76:**8582–8595.
16. **Guidotti, L. G., and F. V. Chisari.** 2006. Immunobiology and pathogenesis of viral hepatitis. Annu. Rev. Pathol. **1:**23–61.
17. **Guo, J. T., V. V. Bichko, and C. Seeger.** 2001. Effect of alpha interferon on the hepatitis C virus replicon. J. Virol. **75:**8516–8523.
18. **Hamamoto, I., Y. Nishimura, T. Okamoto, H. Aizaki, M. Liu, Y. Mori, T. Abe, T. Suzuki, M. M. Lai, T. Miyamura, K. Moriishi, and Y. Matsuura.** 2005. Human VAP-B is involved in hepatitis C virus replication through interaction with NS5A and NS5B. J. Virol. **79:**13473–13482.
19. **Hoofnagle, J. H.** 2002. Course and outcome of hepatitis C. Hepatology **36:**S21–S29.
20. **Ichimura, T., H. Yamamura, K. Sasamoto, Y. Tominaga, M. Taoka, K. Kakiuchi, T. Shinkawa, N. Takahashi, S. Shimada, and T. Isobe.** 2005. 14-3-3 proteins modulate the expression of epithelial Na+ channels by phosphorylation-dependent interaction with Nedd4-2 ubiquitin ligase. J. Biol. Chem. **280:**13187–13194.
21. **Inoue, K., S. Ueno, and A. Fukuda.** 2004. Interaction of neuron-specific K^+-Cl^- cotransporter, KCC2, with brain-type creatine kinase. FEBS Lett. **564:**131–135.
22. **Inoue, K., J. Yamada, S. Ueno, and A. Fukuda.** 2006. Brain-type creatine kinase activates neuron-specific K^+-Cl^- cotransporter KCC2. J. Neurochem. **96:**598–608.
23. **Kato, T., T. Date, M. Miyamoto, A. Furusaka, K. Tokushige, M. Mizokami, and T. Wakita.** 2003. Efficient replication of the genotype 2a hepatitis C virus subgenomic replicon. Gastroenterology **125:**1808–1817.
24. **Kato, T., A. Furusaka, M. Miyamoto, T. Date, K. Yasui, J. Hiramoto, K. Nagayama, T. Tanaka, and T. Wakita.** 2001. Sequence analysis of hepatitis C virus isolated from a fulminant hepatitis patient. J. Med. Virol. **64:**334–339.
25. **Lancaster, A. M., E. Jan, and P. Sarnow.** 2006. Initiation factor-independent translation mediated by the hepatitis C virus internal ribosome entry site. RNA **12:**894–902.
26. **Lillie, J. W., D. F. Smee, J. H. Huffman, L. J. Hansen, R. W. Sidwell, and R. Kaddurah-Daouk.** 1994. Cyclocreatine (1-carboxymethyl-2-iminoimidazolidine) inhibits the replication of human herpesviruses. Antivir. Res. **23:**203–218.
27. **Lindenbach, B. D., M. J. Evans, A. J. Syder, B. Wolk, T. L. Tellinghuisen, C. C. Liu, T. Maruyama, R. O. Hynes, D. R. Burton, J. A. McKeating, and C. M. Rice.** 2005. Complete replication of hepatitis C virus in cell culture. Science **309:**623–626.
28. **Lindenbach, B. D., B. M. Pragai, R. Montserret, R. K. Beran, A. M. Pyle, F. Penin, and C. M. Rice.** 2007. The C terminus of hepatitis C virus NS4A encodes an electrostatic switch that regulates NS5A hyperphosphorylation and viral replication. J. Virol. **81:**8905–8918.
29. **Mahajan, V. B., K. S. Pai, A. Lau, and D. D. Cunningham.** 2000. Creatine kinase, an ATP-generating enzyme, is required for thrombin receptor signaling to the cytoskeleton. Proc. Natl. Acad. Sci. USA **97:**12062–12067.
30. **Mannova, P., R. Fang, H. Wang, B. Deng, M. W. McIntosh, S. M. Hanash, and L. Beretta.** 2006. Modification of host lipid raft proteome upon hepatitis C virus replication. Mol. Cell Proteomics **5:**2319–2325.
31. **Manos, P., and J. Edmond.** 1992. Immunofluorescent analysis of creatine kinase in cultured astrocytes by conventional and confocal microscopy: a nuclear localization. J. Comp. Neurol. **326:**273–282.
32. **Meffert, G., F. N. Gellerich, R. Margreiter, and M. Wyss.** 2005. Elevated creatine kinase activity in primary hepatocellular carcinoma. BMC Gastroenterol. **5:**9.
33. **Miyanari, Y., M. Hijikata, M. Yamaji, M. Hosaka, H. Takahashi, and K. Shimotohno.** 2003. Hepatitis C virus nonstructural proteins in the probable membranous compartment function in viral genome replication. J. Biol. Chem. **278:**50301–50308.
34. **Moradpour, D., F. Penin, and C. M. Rice.** 2007. Replication of hepatitis C virus. Nat. Rev. Microbiol. **5:**453–463.
35. **Muhlebach, S. M., M. Gross, T. Wirz, T. Wallimann, J. C. Perriard, and M. Wyss.** 1994. Sequence homology and structure predictions of the creatine kinase isoenzymes. Mol. Cell Biochem. **133–134:**245–262.
36. **Murakami, K., K. Ishii, Y. Ishihara, S. Yoshizaki, K. Tanaka, Y. Gotoh, H. Aizaki, M. Kohara, H. Yoshioka, Y. Mori, N. Manabe, I. Shoji, T. Sata, R. Bartenschlager, Y. Matsuura, T. Miyamura, and T. Suzuki.** 2006. Production of infectious hepatitis C virus particles in three-dimensional cultures of the cell line carrying the genome-length dicistronic viral RNA of genotype 1b. Virology **351:**381–392.
37. **Nomura-Takigawa, Y., M. Nagano-Fujii, L. Deng, S. Kitazawa, S. Ishido, K. Sada, and H. Hotta.** 2006. Non-structural protein 4A of Hepatitis C virus accumulates on mitochondria and renders the cells prone to undergoing mitochondria-mediated apoptosis. J. Gen. Virol. **87:**1935–1945.
38. **Ohara-Imaizumi, M., T. Fujiwara, Y. Nakamichi, T. Okamura, Y. Akimoto, J. Kawai, S. Matsushima, H. Kawakami, T. Watanabe, K. Akagawa, and S. Nagamatsu.** 2007. Imaging analysis reveals mechanistic differences between first- and second-phase insulin exocytosis. J. Cell Biol. **177:**695–705.
39. **Okamoto, T., Y. Nishimura, T. Ichimura, K. Suzuki, T. Miyamura, T. Suzuki, K. Moriishi, and Y. Matsuura.** 2006. Hepatitis C virus RNA replication is regulated by FKBP8 and Hsp90. EMBO J. **25:**5015–5025.
40. **Oliver, I. T.** 1955. A spectrophotometric method for the determination of creatine phosphokinase and myokinase. Biochem. J. **61:**116–122.
41. **Shi, S. T., K. J. Lee, H. Aizaki, S. B. Hwang, and M. M. Lai.** 2003. Hepatitis C virus RNA replication occurs on a detergent-resistant membrane that cofractionates with caveolin-2. J. Virol. **77:**4160–4168.
42. **Shirakura, M., K. Murakami, T. Ichimura, R. Suzuki, T. Shimoji, K. Fukuda, K. Abe, S. Sato, M. Fukasawa, Y. Yamakawa, M. Nishijima, K. Moriishi, Y. Matsuura, T. Wakita, T. Suzuki, P. M. Howley, T. Miyamura, and I. Shoji.** 2007. E6AP ubiquitin ligase mediates ubiquitylation and degradation of hepatitis C virus core protein. J. Virol. **81:**1174–1185.
43. **Sunahara, Y., K. Uchida, T. Tanaka, H. Matsukawa, M. Inagaki, and Y. Matuo.** 2001. Production of recombinant human creatine kinase (r-hCK) isozymes by tandem repeat expression of M and B genes and characterization of r-hCK-MB. Clin. Chem. **47:**471–476.

Downloaded from jvi.asm.org at National Institute of Infectious Diseases on March 15, 2010

44. **Suzuki, T., K. Ishii, H. Aizaki, and T. Wakita.** 2007. Hepatitis C viral life cycle. Adv. Drug Deliv. Rev. **59:**1200–1212.
45. **Taguwa, S., T. Okamoto, T. Abe, Y. Mori, T. Suzuki, K. Moriishi, and Y. Matsuura.** 2008. Human butyrate-induced transcript 1 interacts with hepatitis C virus NS5A and regulates viral replication. J. Virol. **82:**2631–2641.
46. **Takeuchi, T., A. Katsume, T. Tanaka, A. Abe, K. Inoue, K. Tsukiyama-Kohara, R. Kawaguchi, S. Tanaka, and M. Kohara.** 1999. Real-time detection system for quantification of hepatitis C virus genome. Gastroenterology **116:**636–642.
47. **Wakita, T., T. Pietschmann, T. Kato, T. Date, M. Miyamoto, Z. Zhao, K. Murthy, A. Habermann, H. G. Krausslich, M. Mizokami, R. Bartenschlager, and T. J. Liang.** 2005. Production of infectious hepatitis C virus in tissue culture from a cloned viral genome. Nat. Med. **11:**791–796.
48. **Wallimann, T., M. Wyss, D. Brdiczka, K. Nicolay, and H. M. Eppenberger.** 1992. Intracellular compartmentation, structure and function of creatine kinase isoenzymes in tissues with high and fluctuating energy demands: the 'phosphocreatine circuit' for cellular energy homeostasis. Biochem. J. **281**(Pt. 1)**:**21–40.
49. **Watashi, K., N. Ishii, M. Hijikata, D. Inoue, T. Murata, Y. Miyanari, and K. Shimotohno.** 2005. Cyclophilin B is a functional regulator of hepatitis C virus RNA polymerase. Mol. Cell **19:**111–122.
50. **Wolk, B., D. Sansonno, H. G. Krausslich, F. Dammacco, C. M. Rice, H. E. Blum, and D. Moradpour.** 2000. Subcellular localization, stability, and trans-cleavage competence of the hepatitis C virus NS3-NS4A complex expressed in tetracycline-regulated cell lines. J. Virol. **74:**2293–2304.
51. **Wyss, M., and R. Kaddurah-Daouk.** 2000. Creatine and creatinine metabolism. Physiol. Rev. **80:**1107–1213.
52. **Yi, M., R. A. Villanueva, D. L. Thomas, T. Wakita, and S. M. Lemon.** 2006. Production of infectious genotype 1a hepatitis C virus (Hutchinson strain) in cultured human hepatoma cells. Proc. Natl. Acad. Sci. USA **103:**2310–2315.
53. **Yi, Z., C. Fang, T. Pan, J. Wang, P. Yang, and Z. Yuan.** 2006. Subproteomic study of hepatitis C virus replicon reveals Ras-GTPase-activating protein binding protein 1 as potential HCV RC component. Biochem. Biophys. Res. Commun. **350:**174–178.
54. **Zhong, J., P. Gastaminza, G. Cheng, S. Kapadia, T. Kato, D. R. Burton, S. F. Wieland, S. L. Uprichard, T. Wakita, and F. V. Chisari.** 2005. Robust hepatitis C virus infection in vitro. Proc. Natl. Acad. Sci. USA **102:**9294–9299.

Downloaded from jvi.asm.org at National Institute of Infectious Diseases on March 15, 2010

Arch Virol
DOI 10.1007/s00705-009-0433-6

ORIGINAL ARTICLE

Characterization of anti-idiotypic antibodies mimicking antibody- and receptor-binding sites on hepatitis A virus

Tomoko Kiyohara · Atsuko Totsuka · Tetsuo Yoneyama · Koji Ishii · Toshihiro Ito · Takaji Wakita

Received: 19 December 2008 / Accepted: 12 June 2009
© Springer-Verlag 2009

Abstract Two anti-idiotypic monoclonal antibodies (mAb2s; named 94-2 and 94-7), were generated from a BALB/c mouse immunized with human monoclonal anti-hepatitis A virus (HAV) neutralizing antibody KF94. We characterized the properties of the mAb2s and determined interactions between mAb2s, KF94 and HAV using enzyme-linked immunosorbent assay, immunofluorescence assay and HAV infectivity assay. Inactivated HAV inhibited mAb2 binding to KF94, indicating that the mAb2s mimicked the HAV neutralization site that was complementary to the paratope of KF94. MAb2 94-7 competed with an anti-HAV cellular receptor antibody for binding to HAV-susceptible cells and partially blocked virus infection. We speculated that mAb2 94-7 mimicked a portion of the HAV receptor-binding site. The ability to generate mAb2 implies that HAV receptor-binding sites are exposed on the surface of HAV, permitting antibody access.

Introduction

Hepatitis A virus (HAV) is an epidemiologically important pathogen that causes acute hepatitis in humans [12]. It is a positive-strand RNA virus belonging to the family *Picornaviridae*, genus *Hepatovirus* [16].

Picornavirus particles contain 60 protomers arranged as 12 pentamers. Each protomer is composed of four capsid proteins, viral protein (VP) 1, VP2, VP3 and VP4. The HAV particle also contains 60 protomers, made up of the same capsid proteins, but the VP4 of HAV is truncated and smaller than the VP4 proteins found in other picornaviruses [5].

Unlike other picornaviruses [3], the antigenic structure of HAV has not been completely characterized. Its unique features, the difficulty of obtaining a high virus yield in tissue culture and the strict conformational dependence of its own neutralizing antigenic structure have hampered investigations of HAV morphology. Generating neutralizing antibodies in response to individual structural proteins, synthetic peptides or expressed polypeptides is reportedly difficult [7, 10, 15]. Fragmental structural proteins cannot maintain the function of the neutralizing site. Studies using escape mutants have generated information about the antigenic structure of HAV [17, 19] that supports the notion of an immunodominant neutralizing site involving residues of VP1 and VP3, and that a second, potentially independent site involves residue 221 of VP1.

We generated anti-idiotypic antibodies (anti-Id) by immunization with an HAV-specific human neutralizing monoclonal antibody to investigate the antigenic structure of HAV. Immunization with an antibody (Ab1) can induce anti-antibody antibodies (Ab2s), and those specific for idiotopes of Ab1 are considered anti-Ids. Idiotopes are confined to the variable region of immunoglobulin molecules, and they are crucial for antigen recognition [21]. Among the four known types of anti-Ids (Ab2α, Ab2β, Ab2γ and Ab2ε) [2], Ab2β binds directly to the

T. Kiyohara (✉) · A. Totsuka · T. Yoneyama · K. Ishii · T. Wakita
Department of Virology II, National Institute of Infectious Diseases, 4-7-1, Gakuen, Musashi-Murayama, Tokyo 208-0011, Japan
e-mail: kiyohara@nih.go.jp

T. Ito
Laboratory of Veterinary Public Health, Faculty of Agriculture, Tottori University, 4-101, Minami Koyama, Tottori 680-8553, Japan

Published online: 04 July 2009

idiotope within the paratope of Ab1. Ab2β has the potential to mimic the structure of the antigenic epitope complementary to the Ab1 paratope and it has an antigen-like function. Several reports have used anti-Ids to identify viral/bacterial antigenic structure or cellular receptors [1, 9].

Here, we describe the properties of our anti-Ids, designated mAb2 94-2 and 94-7, which mimic the HAV surface structure and allowed unique insight into the antigenic structure of HAV.

Materials and methods

Cell line and viruses

The GL37 line was derived from African green monkey kidney cells and established to support the optimal growth of HAV [20]. GL37 cells were cultured in Eagle's minimal essential medium (Nissui, Tokyo, Japan) supplemented with 50 μg/ml of gentamicin (Biological Industries, Kibbutz Beit Haemek, Israel) and 10% fetal bovine serum (FBS, GIBCO, Invitrogen Corporation, Auckland, NZ).

Human tissue-culture-adapted hepatitis A virus strains KRM003 (genotype IIIB), KRM031 (genotype IA) and TKM005 (genotype IB) were isolated from patients with hepatitis A [18] and propagated in GL37 cells. Each strain was purified from cell extracts by differential centrifugation, chloroform extraction, RNase, DNase and protein K digestion, extraction with a mixture of 2-ethoxyethanol and 2-buthoxyethanol, and gel filtration. After sucrose gradient centrifugation, the fraction containing intact particles was selected.

The HAV strain KRM003 was propagated and purified as described above. Purified virus was inactivated with 0.025% formalin at 37°C for 12 days and then diluted with 10 mM Tris–HCl, 2 mM EDTA, 100 mM NaCl, 0.02% Tween 80, 0.1% NP40, 0.2% BSA, 0.03% NaN_3 to 3 mg/ml and stored at 4°C.

Preparation of anti-HAV antibodies

Syngeneic anti-HAV human monoclonal antibodies designated KF6 and KF94 provided by Dr. Yasushi Kuwahara, Denka Seiken Co. Ltd. [4] corresponded to Ab1s derived from the blood of a convalescent patient with hepatitis A who was infected with strain IIIB. Here, the parental antibody was KF94, which cross-reacted with a mouse monoclonal antibody that recognized the HAV immunodominant site (data not shown).

Anti-HAV rabbit hyperimmune serum was prepared by immunization with the inactivated HAV.

Generation of mouse monoclonal anti-KF94 antibodies (mAb2s)

Hybridoma clones were selected from the fusion products of SP2/0 myeloma (Riken Cell Bank, Tsukuba, Japan) and spleen cells of BALB/c mice immunized with KF94.

The affinity of culture fluid from each hybridoma clone to KF94 was tested using an enzyme-linked immunosorbent assay (ELISA) (Table 1). Polystyrene microtiter plates (F96 CERT. MAXISORP, Nunc Laboratories, Roskilde, Denmark) were coated with 50 μl of appropriately diluted KF94, or with anti-HAV-negative human serum obtained from a healthy individual. Sera or specimens derived from human sources were collected after obtaining informed consent from the donors.

Nonspecific binding in the wells was blocked with bovine serum albumin. Culture fluid (50 μl) was applied to plates coated with either KF94 or anti-HAV-negative human serum. Bound antibody was detected by incubation with a horseradish-peroxidase-conjugated (HRPO) anti-mouse IgG (MBL, Nagoya, Japan) followed by *o*-phenylenediamine (Tokyo Chemical Industry Co, Ltd, Tokyo, Japan) substrate. Thirty minutes later, the reaction was stopped with 2 N H_2SO_4. Absorbance was measured at 492 nm in an ELISA plate reader (Corona, Hitachinaka, Japan). The procedures for color development and absorbance measurement subsequent to adding conjugated antibody were identical in every subsequent ELISA.

Antibodies that reacted with KF94 and not with anti-HAV-negative human serum were identified as KF94-specific mAb2s. The isotype of the mAb2 was determined using a mouse monoclonal antibody isotyping test kit (Serotec Ltd., Oxford, UK). The ascitic fluid of each mAb2 was obtained by intraperitoneal injection of hybridomas into pristane-primed BALB/c mice. Animals were handled and cared for in accordance with the "Guidelines for Animal Experimentation at NIID."

Cross-reactivity between the selected mAb2s was determined by competitive inhibition ELISA using biotin-labeled mAb2s and KF94-coated plates (Table 1). Briefly, non-labeled mAb2 was applied to KF94-coated plates, followed by biotin-labeled specific or non-specific mAb2. The mAb2 was labeled with biotin using EZ-Link NHS-Biotin (Pierce, Rockford, IL, USA) according to the manufacturer's instructions and detected using HRPO avidin (MBL, Nagoya, Japan).

Biotin-labeled mAb2s were also used in mAb2-HAV binding ELISA (Table 1). Serially diluted biotin-labeled mAb2s were applied to plates that were prepared as follows: polystyrene microtiter plates were coated with 50 μl of anti-HAV rabbit hyperimmune serum, and nonspecific binding was blocked with bovine serum albumin. Fifty microliters of formalin-inactivated HAV strain KRM003

Table 1 Summary of ELISA used in this study

Aim of ELISA	Plate coated with	First input	Second input	Third input
MAb2-KF94 binding	KF94	MAb2	HRPO anti-mouse IgG	–
MAb2 cross reactivity	KF94	MAb2	Biotin-labeled mAb2s	HRPO avidin
MAb2-HAV binding	Anti-HAV rabbit hyperimmune serum[a]	Inactivated HAV	Biotin-labeled mAb2s	HRPO avidin
Inhibition of binding of Ab1 to HAV by mAb2	Anti-HAV rabbit hyperimmune serum[a]	Inactivated HAV	The mixture of Ab1 and mAb2	HRPO anti-human IgG
Inhibition of binding of KF94 to mAb2 by HAV	KF94	Inactivated HAV	Biotin-labeled mAb2s	HRPO avidin
Competitive inhibition	GL37 cells	MAb2s	HRPO anti-HAV receptor antibody 190/4C	–

[a] We confirmed that anti-HAV rabbit hyperimmune serum did not bind to mAb2s

(20 ng/ml) was added, and the plates were incubated overnight at 4°C. Bound biotin-labeled mAb2s were detected as described above.

Inhibition assays

We determined the ability of the mAb2 to inhibit the binding of KF94 to HAV (Table 1). A mixture of diluted Ab1 and mAb2 was incubated at 4°C overnight and then applied to HAV-coated plates. Bound Ab1 was detected using a HRPO anti-human IgG (Dako, Glostrup, Denmark).

We examined the ability of inactivated HAV to inhibit the binding of KF94 to mAb2 (Table 1). Serially diluted inactivated HAV was incubated in KF94 plates overnight at 4°C, and then the wells were emptied. Biotin-labeled mAb2 (diluted 1:1,000) was applied to the wells, followed by HRPO avidin. Inhibition rates were measured using the formula:

Inhibition rate (%) = 100 × (absorbance without inhibitor − absorbance with inhibitor)/absorbance without inhibitor.

Anti-HAV-cellular-receptor mouse monoclonal antibodies

Anti-HAV-cellular-receptor mouse monoclonal antibodies (anti-HAV-receptor antibodies), designated 190/4, 235/4 and 263/6, were induced by immunizing GL37 cells and selected by their ability to block HAV propagation in GL37 cells [11]. We confirmed that the anti-HAV receptor antibodies recognized a common receptor. Anti-HAV receptor antibody190/4 was conventionally conjugated with horseradish peroxidase and named 190/4C.

Binding of mAb2 to HAV cellular receptor

The binding of each mAb2 to GL37 cells was examined using an immunofluorescence assay. The positive controls were the anti-HAV-receptor antibodies, 190/4, 235/4 and 263/6, and the negative control was a normal mouse serum (NMS) that was confirmed to be negative for anti-HAV antibody.

Confluent, unfixed GL37 cell monolayers on glass cover slips were gently washed with phosphate-buffered saline (PBS) and then incubated with mAb2 or control antibodies for 1 h at 37°C in a moist chamber. The cover slips were washed with PBS and then incubated with fluorescently labeled anti-mouse IgG (MBL, Nagoya, Japan) for 1 h at 37°C in a moist chamber. The labeled anti-mouse IgG was removed, and the cover slips were washed three times in PBS. The cell surface was immediately observed using a fluorescence microscope.

We confirmed using competitive inhibition ELISA that mAb2 94-7 and anti-HAV receptor antibody 190/4 shared the same HAV cellular receptors.

The anti-HAV receptor antibody 235/4 was the positive competitor, and an anti-human Fc mouse monoclonal antibody (anti-human Fc mAb) was the negative competitor in this ELISA. An anti-human Fc mAb bound non-specifically to KF94 despite being simultaneously generated with the mAb2s 94-2 and 94-7.

Confluent GL37 cell monolayers in 96-well cell culture plates (Corning, NY, USA) were incubated with serially diluted mAb2s and positive or negative competitors for 2 h at 37°C. After washing with PBS, 50 µl of HRPO anti-HAV-receptor antibody 190/4C was added to the corresponding wells and incubated for 2 h at 37°C. The wells were washed, and then bound HRPO anti-HAV receptor antibody was detected. Competition rates were measured using the formula:

Competition rate (%) = 100 (absorbance without competitor − absorbance with competitor)/absorbance without competitor.

Infectivity assays

We performed $TCID_{50}$-infectivity and immunofocus assays to investigate the mAb2-mediated protection of GL37 cells against HAV infection.

For $TCID_{50}$-infectivity assays, GL37 cell monolayers in 96-well cell culture plates were incubated with 50 µl of serially diluted mAb2 for 1 h at 37°C in a CO_2 incubator. Without washing, 25 µl of HAV, genotype IA, IB or IIIB, was added to the appropriate wells and incubated for 1 h at 37°C. Cells were infected with all HAVs at a multiplicity of infection of 100. Infected cells were maintained in Eagle's minimal essential medium (EMEM) supplemented with 2 mM L-glutamine, 50 µg/ml of gentamicin, 2% fetal bovine serum and 0.15% of sodium bicarbonate (2% FBS-EMEM) for 3 days. Infected cells were fixed with 80% methanol containing 0.03% H_2O_2, and air-dried, and then HAV propagated in infected cells was detected using anti-HAV hyperimmune rabbit serum. The plates were washed and incubated with HRPO anti-rabbit IgG (MBL, Nagoya, Japan), and then the rate of blocking of infection was measured using the formula:

Blocking rate (%) = 100 × (absorbance without inhibitor − absorbance with inhibitor)/absorbance without inhibitor.

The immunofocus assay was a modified radioimmunofocus assay [13] as follows: We mixed 50 µl of mAb2 (diluted 1:20 in PBS supplemented with 2% FBS) with an equal volume of HAV, genotype IA, IB or IIIB, containing 40–60 focus-forming units (FFU) in 2% FBS-EMEM. GL37 cell monolayers in six-well cell culture plates (Falcon, Franklin Lakes, NJ, USA) were inoculated with 100 µl of the mAb2-HAV mixture and incubated for 1 h at 37°C in a 5% CO_2 environment to allow mAb2 and virus adsorption to the cells. Without removing the inoculum, the GL37 monolayer was overlaid with 5 ml of Dulbecco's modified Eagle medium (Nissui, Tokyo, Japan) containing 0.6% agarose ME (Iwai Chemicals Company, Tokyo, Japan), 2% FBS and 0.22% sodium bicarbonate. After the agar had solidified, the cultures were placed upside down and incubated at 37°C for 10–12 days at 37°C in 5% CO_2. The agarose overlay was discarded, and the cells were fixed with 1.5 ml of 80% methanol containing 0.03% H_2O_2 for 1 h at 4°C. Anti-HAV rabbit hyperimmune serum (1 ml of 1:2,000 dilution) was added to each well and incubated overnight at 4°C. The wells were washed with PBS and then incubated with 1 ml of HRPO anti-rabbit IgG for 2 h at 37°C. The plates were washed once again, and then HAV foci were detected using 1.5 ml of DAB substrate [0.5 mg/ml diaminobenzidine, 0.03% $(NH_4)_2Ni(SO_4)_2$, 0.03% $CoCl_2$, 0.03% H_2O_2 in PBS]. Infection was considered blocked if the input FFU was reduced by ≥50%.

Results

Binding properties of mAb2s

Among the hybridoma clones secreting mAb2, two stable clones were selected by KF94-binding ELISA. The ascitic fluids of the selected clones, designated mAb2 94-2 and 94-7 were specific for KF94, and they did not react with either KF6 or HAV-negative human serum. The titers of mAb2 94-2 and 94-7, given as the reciprocal of the end-point dilution required to generate maximal absorbance in KF94-binding ELISA, were 102,400 and 25,600, respectively. Both were categorized as IgG1 subclass, κ chain. They did not cross-react or bind to HAV.

Interactions between mAb2s, KF94 and HAV

Figure 1a shows that both mAb2s inhibited KF94 binding to HAV. At a 1:1,000 dilution, mAb2 94-2 and 94-7

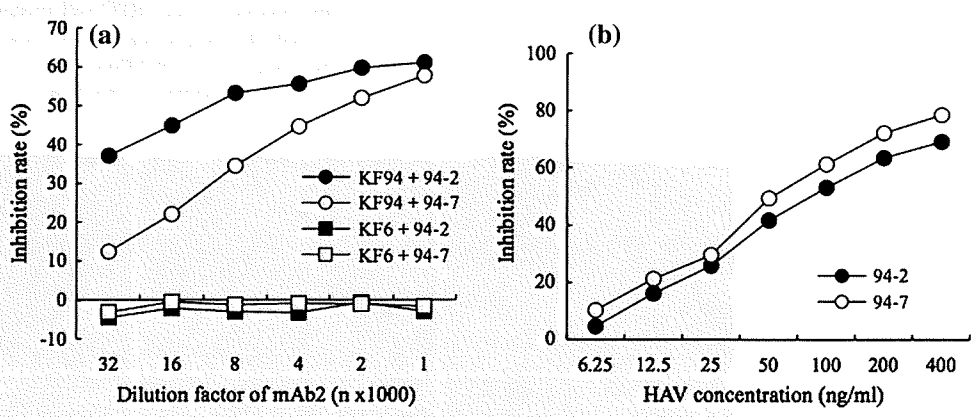

Fig. 1 Interactions between KF94, mAb2s and HAV. Anti-HAV antibodies KF6 and KF94 were incubated with serially diluted mAb2 94-2 or 94-7 (*filled circle*, KF94 and 94-2; *open circle*, KF94 and 94-7; *filled square*, KF6 and 94-2; *open square*, KF6 and 94-7; **(a)**, and then binding to inactivated HAV was determined by ELISA. The mAb2s (diluted 1:1,000) inhibited KF94 binding to HAV by 60%. The mAb2s did not interfere with KF6 binding to HAV, thus confirming their specificity. Anti-HAV antibody KF94 was incubated with serially diluted inactivated HAV, and binding of preincubated KF94 to mAb2 94-2 (*filled circle*) or 94-7 (*open circle*) was determined by ELISA. Inactivated HAV interfered with mAb2 binding to KF94 **(b)**

inhibited 61.1 and 57.7% of the binding, respectively, and the inhibition rate gradually decreased with higher dilutions. The inhibition ability was specific for KF94. The mAb2s did not affect anti-HAV human mAb KF6 binding to HAV.

Inactivated HAV inhibited KF94 binding to mAb2s (Fig. 1b). The inhibition rates were proportional to the concentration of inactivated HAV. KF94 binding to the mAb2s 94-2 and 94-7 was inhibited by 69.1 and 78.5%, respectively, at the maximal concentration of inactivated HAV. Binding of mAb2s or HAV to KF94 reduced the affinity of KF94.

Binding of mAb2 to HAV cellular receptor

Binding of mAb2 94-7 and anti-HAV receptor antibodies 190/4, 235/4, and 263/6 to GL37 cells was confirmed by immunofluorescence staining (Fig. 2). Neither mAb2 94-2 nor NMS bound to GL37 cells.

We performed competitive inhibition ELISA to confirm that mAb2 94-7 and anti-HAV receptor antibody shared the same HAV cellular receptor. Anti-HAV receptor antibody 235/4 and mAb2 94-7 competed with the HRPO anti-HAV receptor 190/4C for binding to HAV cellular receptors. Figure 3 shows that the inhibition rates were proportional to the concentrations of the competitors. At a 1:100 dilution, the inhibition rates of the positive competitor, mAb2 94-7 and 94-2, and the negative competitor were 93.2, 59.2, 20.8 and 18.5%, respectively. The inhibition rate of mAb2 94-7 was lower than that of the anti-HAV-receptor antibody 235/4, but higher than that of the mAb2 94-2 or the negative competitor.

MAb2-mediated protection of GL37 cells from HAV infection

The rates of mAb2 94-7-mediated blocking of GL37 cell infection with HAV in $TCID_{50}$-infectivity assays were 65.8, 54.1, and 86.0% for genotypes IA, IB, and IIIB, respectively. Blocking rates are expressed as dose-response curves (Fig. 4). On the other hand, mAb2 94-2 enhanced HAV propagation rather than protecting the cells.

Immunofocus assays showed that the number of immunofoci of genotype IIIB strain KRM003 was reduced by 83.3% in the presence of mAb2 94-7 diluted 1:40. The results were similar for genotypes IA and IB, which reduced the number of immunofoci by 71.1 and 77.8%, respectively, at the same dilution. In contrast, mAb2 94-2 did not reduce the numbers of immunofoci.

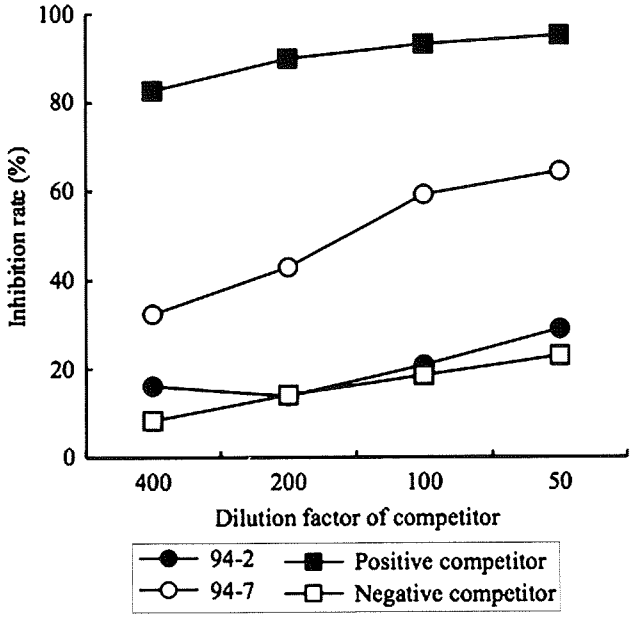

Fig. 3 Binding of mAb2s to GL37 cells in competition with anti-HAV receptor antibody. Positive competitor (*filled square*) and mAb2 94-7 (*open circle*) interfered with HRPO anti-receptor antibody 190/C binding to GL37 cells by recognizing the common HAV receptors of GL37 cells. The competitive inhibition rates of mAb2 94-2 (*filled circle*) and of negative competitor (*open square*) were equally low

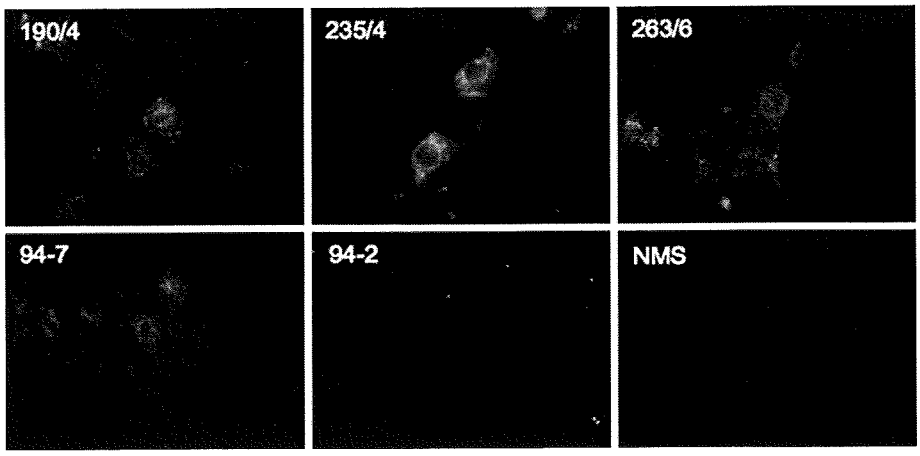

Fig. 2 Binding of mAb2s to GL37 cells. MAb2 94-7 and anti-receptor antibodies (190/4, 235/4 and 263/6) bound to GL37 cells were detected by immunofluorescence assay. MAb2 94-2 and normal mouse serum (*NMS*) were undetectable

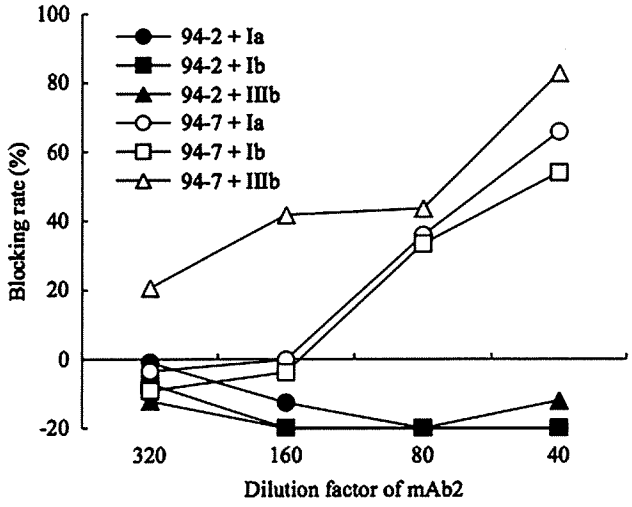

Fig. 4 MAb2-mediated protection of GL37 cells from HAV infection determined by $TCID_{50}$-infectivity assay. GL37 cells were protected from HAV infection by mAb2 94-7, but not by mAb2 94-2. Combinations of mAb2 and HAV genotypes: *filled circle* 94-2 and IA; *filled square* 94-2 and IB; *filled triangle*, 94-2 and IIIB; *open circle*, 94-7 and IA; *open square*, 94-7 and IB; *open triangle*, 94-7 and IIIB

Discussion

We generated the anti-idiotypic antibodies mAb2 94-2 and 94-7 by immunizing a mouse with anti-HAV neutralizing antibody KF94. The mAb2s were specific for the parental anti-HAV antibody KF94 and did not cross-react. They inhibited the binding of KF94 to HAV (Fig. 1a), and inactivated HAV competitively inhibited the binding of KF94 to the mAb2s (Fig. 1b), suggesting that the mAb2s and HAV bound to the paratope of KF94. Each mAb2 recognized different idiotopes within the paratope and could bind to KF94 as a surrogate of HAV.

These data indicated that the mAb2s mimic an HAV neutralization site that is complementary to the paratope of KF94. However, mimicry of the neutralization site by mAb2s might be incomplete, because the mAb2s inhibited KF94-HAV binding by only about 60%.

The characteristics of the mAb2s differed with respect to their affinity for the HAV-susceptible cell line GL37. The mAb2 94-2 neither bound to GL37 cells (Fig. 2) nor inhibited HAV infection (Fig. 4). The mAb2 94-2 seemed to have mimicked a portion of the antibody-binding site in the HAV neutralization site. The mimicked antibody-binding site interfered with KF94-HAV binding but did not influence virus-cellular receptor interaction.

On the other hand, mAb2 94-7 competed with the anti-HAV-cellular-receptor antibodies for binding to GL37 cells (Figs. 2, 3). The binding of mAb2 94-7 to GL37 cells partially blocked HAV infection (Fig. 4). We postulate that the mAb2 94-7 mimicked the part of the neutralization site that contains functional antibody-binding and cellular-receptor-binding sites.

The speculation that mimicry of the HAV neutralization site by mAb2 would be incomplete also explains why mAb2 94-7 could not totally block HAV infection. MAb2 94-7 was capable of blocking the infectivity of different genotypic strains (Fig. 4) and thus seems to mimic a common receptor-binding site among genotypes IA, IB and IIIB. Thus, these genotype strains might infect GL37 cells via a common receptor. Among the three genotypes, the rate at which mAb2 94-7 blocked infection was highest against strain IIIB (Fig. 4), which might be because KF94 was prepared from a patient infected with HAV strain IIIB.

Anti-idiotypic antibodies induced by immunization with an anti-Sindbis-virus neutralizing antibody competed with the virus for cellular receptors [22]. This suggested that a crucial receptor-binding site exposed on the viral surface is recognized by Ab1. We also speculate that the HAV receptor-binding site is exposed on the viral surface, because mAb2 94-7 competed with HAV for cellular receptors. Furthermore, the syngeneic mAb2 94-2 mimics part of the antibody-binding site. These data indicate that the antibody- and receptor-binding sites mimicked by mAb2s are exposed on the viral surface and are in close vicinity or overlap, thus comprising an epitope that could induce KF94.

Unlike other members of the family *Picornaviridae* [3], very little is understood about HAV neutralization sites and relationships between antibody- and receptor-binding sites. However, all published data support the notion that major and minor immunodominant neutralization sites exist on HAV virions and empty capsids [17, 19]. The immunodominant neutralization sites of native particles appear to be conformational and generally differ from those of denatured particles or isolated HAV structural proteins. Antibodies elicited by immunization with native or formalin-inactivated virus have broad neutralizing activity against different strains [20]. In contrast, the development of neutralizing antibodies in response to individual structural proteins, synthetic peptides, or expressed uncleaved precursors and polypeptides is problematic [7, 10, 15]. Thus, analysis of HAV neutralization sites using such probes is not simple. Analysis of HAV neutralization sites has mainly depended on the use of neutralization-escape mutants generated by serial passage of the virus in cultured cells in the presence of neutralizing mouse monoclonal antibodies [17, 19]. Although HAV strains isolated from various parts of the world belong to a single serotype [18], neutralization-escape mutants can be produced experimentally. These mutants are expected to possess a replicative advantage and survive more efficiently than wild-type virus as a result of the arrangement of surface neutralizing antibody-binding sites. However,

their in vivo replication is restricted compared with wild-type virus, although they appear to be equally stable in vitro [14]. Furthermore, although the rate of substitution throughout the HAV genome is high, most of the mutations are silent [6]. Presumably, alterations in neutralizing-antibody-binding sites, such as in neutralization-escape mutants, might arise during natural infection. However, constraints probably prevent this from occurring in nature. Our results indicated that one such constraint depends on the relationship between antibody- and receptor-binding sites on the viral surface. These sites might be closely located or overlap within an immunodominant neutralization site. Therefore, mutations on the antibody-binding site might result in deterioration of the receptor-binding site. Such deterioration would consequently reduce the affinity of the HAV receptor-binding site, which would result in neutralization escape mutants being unable to replicate to significant levels in vivo. Alterations in antibody-binding sites of poliovirus are thought to be responsible for the affinity of the receptor-binding site [8]. The relationship between the antibody- and receptor-binding sites shown by mAb2s might partly explain why only one serotype of HAV exists.

To our knowledge, we are the first to analyze the HAV surface using anti-Ids to mimic receptor- and antibody-binding sites within HAV neutralizing sites. Our anti-Ids could not completely mimic the viral surface structure, but they remained functionally intact. Anti-Id antibodies may be considered obsolete, but they nevertheless represent an effective tool with which to structurally analyze the viral surface.

Acknowledgments The authors would like to thank Dr. Hiroshi Yamamoto and Dr. Yasuo Moritsugu for important suggestions regarding this study.

References

1. Bona CA (1998) Idiotype vaccines: forgotten but not gone. Nat Med 4:668–669
2. Bona CA, Kohler H (1984) Anti-idiotypic antibodies and internal images. In: Venter JC, Fraser CM, Lindstrom J (eds) Monoclonal and anti-idiotypic antibodies: probes for receptor structure and function. Alan R Liss inc, New York, pp 141–149
3. Che Z, Olson NH, Leippe D et al (1998) Antibody-mediated neutralization of human rhinovirus 14 explored by means of cryoelectron microscopy and X-ray crystallography of virus-Fab complexes. J Virol 72:4610–4622
4. Chiba J (1988) A strategy for the production of human monoclonal antibodies. Hum Cell 1:31–36
5. Coulepis AG, Locarnini SA, Gust ID (1980) Iodination of hepatitis A virus reveals a fourth structural polypeptide. J Virol 35:572–574
6. Garcia-Aguirre L, Cristina J (2008) Analysis of the full-length genome of hepatitis A virus isolated in South America: heterogeneity and evolutionary constraints. Arch Virol 153:1473–1478
7. Gauss-Muller V, Deinhardt F (1988) Immunoreactivity of human and rabbit antisera to hepatitis A virus. J Med Virol 24:219–228
8. Harber J, Bernhardt G, Lu H-H et al (1995) Canyon rim residues, including antigenic determinants, modulate serotype-specific binding of polioviruses to mutants of the poliovirus receptor. Virology 214:559–570
9. Hiernaux JR (1988) Idiotypic vaccines and infectious diseases. Infect Immun 56:1407–1413
10. Hughes JV, Stanton LW (1979) Isolation and immunizations with hepatitis A viral structural proteins: induction of antiprotein, antiviral, and neutralizing responses. J Virol 55:395–401
11. Kaplan G, Totsuka A, Thompson P et al (1996) Identification of a surface glycoprotein on African green monkey kidney cells as a receptor for hepatitis A virus. EMBO J 15:4282–4296
12. Kiyohara T, Satoh T, Totsuka A et al (2007) Shifting seroepidemiology of hepatitis A in Japan, 1973–2003. Microbiol Immunol 51:185–191
13. Lemon SM, Binn LN, Marchwicki RH (1983) Radioimmunofocus assay for quantitation of hepatitis A virus in cell cultures. J Clin Microbiol 17:834–839
14. Lemon SM, Binn LN, Marchwicki R et al (1990) In vivo replication and reversion to wild type of a neutralization-resistant antigenic variant of hepatitis A. J Infect Dis 161:7–13
15. Mattioli S, Imberti L, Stellini R et al (1995) Mimicry of the immunodominant conformation-dependent antigenic site of hepatitis A virus by motifs selected from synthetic peptide libraries. J Virol 69:5294–5299
16. Melnick JL (1995) History and epidemiology of hepatitis A virus. J Infect Dis 171(Suppl 1):s2–s8
17. Ping L-H, Lemon SM (1992) Antigenic structure of human hepatitis A virus defined by analysis of escape mutants selected against murine monoclonal antibodies. J Virol 66:2208–2216
18. Robertson BH, Jansen RW, Khanna B et al (1992) Genetic relatedness of hepatitis A virus strains recovered from different geographical regions. J Gen Virol 73:1365–1377
19. Stapleton JT, Lemon SM (1987) Neutralization escape mutants define a dominant immunologic neutralization site on hepatitis A virus. J Virol 61:491–498
20. Totsuka A, Moritsugu Y (1994) Hepatitis A vaccine development in Japan. In: Nishioka K, Suzuki H, Mishiro S et al (eds) Viral hepatitis and liver disease. Springer, Tokyo, pp 509–513
21. Uytdehaag FGCM, Bunschoten H, Ket Weijer et al (1986) From Jenner to Jerne: towards idiotype vaccines. Immunol Rev 90:93–113
22. Wang K-S, Schmalgohn AL, Kuhn RG et al (1991) Antiidiotypic antibodies as probes for the Sindbis virus receptor. Virology 181:694–697

Journal of Medical Virology 81:1513–1516 (2009)

An In-House-Anti-Hepatitis A Virus (HAV)-Specific Immunoglobulin M Capture Enzyme-Linked Immunosorbent Assay: Evaluation and Application to an HAV Outbreak

Tomoko Kiyohara,[1]* Yoshimi Ouchi,[2] Yoshiko Hasegawa,[2] Tomoko Sato,[1] Tetsuo Yoneyama,[1] Koji Ishii,[1] Toshihiro Ito,[3] and Takaji Wakita[1]

[1]*Department of Virology II, National Institute of Infectious Diseases, Tokyo, Japan*
[2]*Shiga Prefectural Institute of Public Health, Otsu, Japan*
[3]*Faculty of Agriculture, Laboratory of Veterinary Public Health, Tottori University, Tottori, Japan*

An anti-hepatitis A virus (HAV)-specific immunoglobulin M capture enzyme-linked immunosorbent assay (anti-HAV IgM ELISA) kit was re-designed for laboratory use and compared with a commercial anti-HAV IgM detection system using 58 serum samples collected from patients, vaccines, and healthy individuals. Because concordance between the two systems was high ($r = 0.93$, $P < 0.05$), 19 sets of serum and fecal samples obtained from individuals exposed to an HAV outbreak were also examined. Serum levels of anti-HAV IgM were determined using the in-house ELISA kit and the HAV genome in fecal samples was detected using the polymerase chain reaction (PCR). Among the 19 sets of sample, 14 were positive for both anti-HAV IgM and the HAV genome. All of those whose serum samples were anti-HAV IgM negative were also negative for the HAV genome in fecal samples. The results of the in-house IgM ELISA were consistent with those of the HAV genome detected by PCR and with the commercial IgM ELISA. The in-house anti-HAV IgM ELISA kit was therefore proven suitable for laboratory use and applicable to epidemiological studies of HAV infection. ***J. Med. Virol. 81:1513–1516, 2009.*** © 2009 Wiley-Liss, Inc.

KEY WORDS: HAV; IgM; outbreak; symptom

INTRODUCTION

Anti-hepatitis A virus (HAV) immunoglobulin M (IgM) is detectable when hepatitis A patients become symptomatic. Titers increase during acute infection [Stapleton, 1995] and anti-HAV IgM typically disappears within 3 months of the initial appearance of symptoms. Anti-HAV immunoglobulin G (IgG) is the major class of antibody generated during convalescence, which suggests that IgG is the primary defense against re-infection [Fiore, 2004; Iino, 2004]. The combination of anti-HAV IgM antibody and total anti-HAV antibody (HAV-specific IgG, IgM, and IgA) differentiates current and past HAV infection. Anti-HAV IgM is important for confirming a diagnosis of acute HAV infection, since acute hepatitis A is clinically indistinguishable from other forms of acute viral hepatitis.

Routine clinical serological specimens are mostly assayed using automated analyzers or other equipment. Commercial anti-HAV IgM antibody detection systems are not necessarily convenient for clinical applications such as high-throughput primary screening.

In this study, an in-house anti-HAV IgM enzyme-linked immunosorbent assay (ELISA) based on a conventional 96-well ELISA format was evaluated in comparison with a commercial anti-HAV IgM detection system by measuring anti-HAV IgM antibody in clinical samples, and the application to HAV outbreak samples was determined.

MATERIALS AND METHODS

IgM in serum samples diluted 1:10,000–1:16,000 was captured on the surface of microtiter plates coated with a specific anti-human IgM antibody (A0425; Dako Cytomatic, Glostrup, Denmark) for the in-house ELISA. Unbound serum was removed by rinsing the plates with washing buffer (phosphate-buffered saline containing

Grant sponsor: Grants-in-Aid for Scientific Research from the Ministry of Health, Labor and Welfare, Japan (from the Research on Food Safety).

*Correspondence to: Tomoko Kiyohara, 4-7-1, Gakuen, Musashi-murayama 208-0011, Tokyo, Japan.
E-mail: kiyohara@nih.go.jp

Accepted 19 May 2009
DOI 10.1002/jmv.21578
Published online in Wiley InterScience (www.interscience.wiley.com)

© 2009 WILEY-LISS, INC.

WILEY InterScience® DISCOVER SOMETHING GREAT

0.05% Tween-20). Captured HAV-specific antibodies were detected by adding 50 µl inactivated HAV antigen (25 ng/ml) followed by an equal volume of appropriately diluted horseradish peroxidase-labeled anti-HAV rabbit polyclonal antibody.

The HAV antigen was inactivated in essentially the same manner that is used to prepare inactivated hepatitis A vaccine [Totsuka and Moritsugu, 1994]. In brief, HAV strain KRM003G72 (Genotype IIIB) was isolated and propagated in cultured African green monkey kidney cells (GL37). The virus was then purified from cell extracts by differential centrifugation, chloroform extraction, RNase and DNase digestion, protein K treatment, and extraction with a mixture of 2-ethoxyethanol and 2-buthoxyethanol followed by gel filtration. Complete viral particles fractionated by sucrose gradient centrifugation were inactivated in 0.025% formalin at 37°C for 12 days, diluted in 10 nM Tris–HCl (pH 7.5), 2 mM EDTA, 100 nM NaCl, 0.02% Tween-80, 0.1% NP-40, 0.2% bovine serum albumin, and 0.03% NaN_3, and stored at 4°C.

An anti-HAV rabbit polyclonal antibody prepared by immunizing a rabbit with inactivated HAV was conjugated with horseradish peroxidase and detected using *o*-phenylenediamine substrate. The reaction was stopped with 2 N H_2SO_4, and plates were read at 492 nm using a reference filter (630 nm).

This assay calculates results based on the ratio of the optical density (OD) to the cutoff OD (S/CO) for each sample and control. The positive control was serum from a patient with hepatitis A (anti-HAV seroconversion panel: PHT902-03, Boston Biomedica, Inc., Bridgewater, MA), 2.9 S/CO measured by the IMx-system (Abbott Laboratories, Abbott Park, IL):

$$\text{Cutoff OD} = \frac{\text{positive control OD}}{2.9}$$

$$\frac{\text{S}}{\text{CO}} = \frac{\text{sample OD}}{\text{cutoff OD}}$$

S/CO criteria: <0.20, negative; 0.20–1.20, equivocal, convalescence; >1.20, positive.

The in-house ELISA was evaluated by using 77 serum samples from a seroconversion panel (5 banked sera from a patient), as well as from 3 patients with acute hepatitis (collected three times each, for a total of 9 samples), 19 individuals receiving hepatitis A vaccination, 25 healthy volunteers, and 19 individuals exposed to an HAV outbreak, as described below.

All 77 serum samples were tested repeatedly using the in-house ELISA, and the results were consistently identical. The sample panel consisted of: (a) 5 serum samples from an anti-hepatitis A seroconversion panel (PHT902, Boston Biomedica, Inc.) comprising a group of serial bleeds from an individual plasma donor during hepatitis A seroconversion (the attached data sheet provides the results from the commercial IMx-system developed by Abbott Laboratories, which was used as a reference assay in this study); (b) serial sera obtained independently from three patients with hepatitis A at three different times for a total of 9 samples (all samples were anonymous except for the date of bleeding and the IMx results); (c) 19 serum samples from individuals vaccinated against hepatitis A obtained 7 months after the first vaccination. Total anti-HAV antibody in all samples was detected by inhibition ELISA as described previously [Kiyohara et al., 2007]. All samples were positive for total anti-HAV antibody. However, because the samples were collected 7 months after the first vaccination, they should have been positive for IgG but negative or low for IgM; (d) 25 serum samples from healthy individuals. All samples in this group were confirmed as negative for total HAV antibody. Samples from groups (c) and (d) were collected after obtaining written informed consent from the participants and the study protocol was approved by the Ethics Committee at the National Institute of Infectious Diseases; (e) 19 sets of serum and fecal samples obtained from individuals exposed to an outbreak of HAV infection caused by food served in a restaurant in Shiga prefecture [Hasegawa et al., 2007]. Both serum and fecal samples were collected within several days of symptom onset. Serum samples from this group were examined using the in-house anti-HAV IgM and total anti-HAV antibody inhibition ELISAs. Conventional real-time polymerase chain reaction (RT-PCR) detected HAV in fecal samples at the Shiga Prefectural Institute of Public Health [Hasegawa et al., 2007]. All samples in group (e) were anonymous except for age and clinical data.

RESULTS

Figure 1 shows the time courses of S/CO of the serial samples in groups (a) and (b). The S/CO ratios of all samples during the early stage of illness were interpreted as IgM-positive. The IgM levels gradually

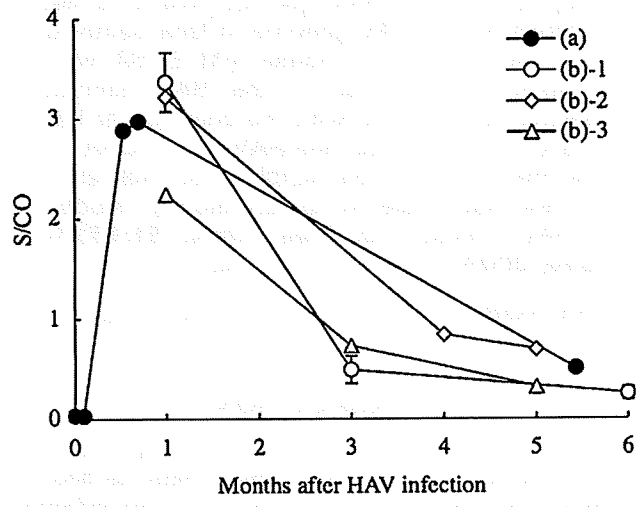

Fig. 1. Time course of anti-HAV IgM antibody in patients with hepatitis A. Serial samples from four patients tested using the in-house anti-HAV IgM ELISA. Serial sample (a) consisted of five sera. Serial samples (b)-1, (b)-2, and (b)-3 belonged to sample group (b), and each sample consisted of three sera. Serial sample (b)-1 was measured five times, and the standard deviation for each serum sample is shown as error bars.

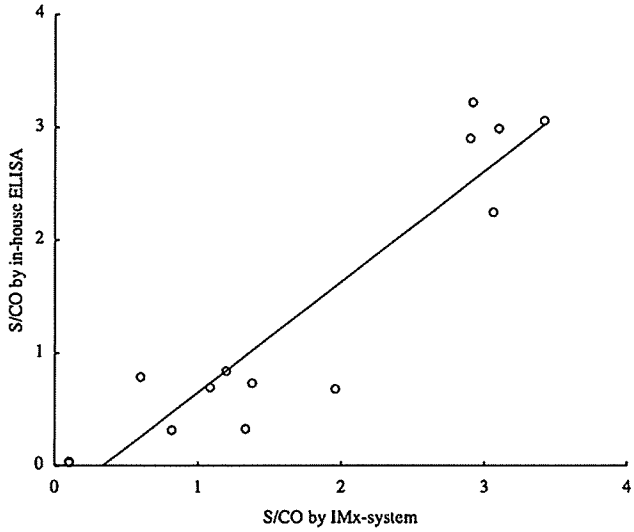

Fig. 2. Correlation between in-house anti-HAV IgM ELISA and IMx results. S/CO ratios of samples in group (a) and (b) are plotted as regression line. Results of both assays closely correlate ($r = 0.93$, $P < 0.05$).

fell over 5 months when the S/CO ratios were interpreted as being at convalescence level.

The results of the in-house ELISA and IMx-system closely agreed ($r = 0.93$, $P < 0.05$), especially in the negative and positive ranges. The in-house ELISA tended to generate smaller S/CO ratios in the middle range than the IMx-system (Fig. 2). All S/CO ratios of samples including groups (c) and (d) were interpreted as IgM-negative. The geometric means of the S/CO ratios of groups (c) and (d) were 0.12 and 0.03, respectively.

Serum samples from group (e) were examined using the in-house anti-HAV IgM and total anti-HAV antibody inhibition ELISAs, and the HAV genome in fecal samples from this group was detected by conventional RT-PCR (Table I). Among 19 individuals, patients 1–14 were positive for both the HAV genome and anti-HAV IgM. All of those whose fecal samples were negative for the HAV genome (patients 15–19) were also negative for anti-HAV IgM. The results of HAV genome detection and the in-house IgM ELISA were consistent. Among those who were anti-HAV IgM negative, patients 18 and 19 were positive for total anti-HAV with titers of 3.58 and 4.10 log10 mIU/ml, respectively.

The symptoms of all individuals were essentially the same and not typical of hepatitis, except for one instance of jaundice (underlined in Table I).

DISCUSSION

An in-house IgM ELISA was designed for laboratory use, and its sensitivity and specificity were compared with those of the IMx-system, which is a commercial anti-HAV IgM detection kit.

The in-house IgM ELISA was highly sensitive and specific for anti-HAV IgM (Figs. 1 and 2). Figure 2 shows that the S/CO ratios measured by the in-house ELISA tended to be smaller in the middle range than those obtained by the IMx-system, suggesting that the in-house ELISA is less sensitive in this range than the IMx-system. However, the in-house ELISA generated fewer false positive results.

Until recently, viral RNA detection was considered impractical for diagnosis because the test was complex, expensive, and insensitive [Stapleton, 1995]. However, improvements in RNA detection technology have led to fecal HAV genome detection becoming routine laboratory confirmation of HAV infection [Yotsuyanagi, 2004]. Fecal shedding is maximal immediately before or soon after the onset of liver failure and can persist for months after symptoms are resolved [Fiore, 2004]. Anti-HAV IgM and the HAV genome (Table I) were

TABLE I. Summary of Clinical Samples Collected During a Hepatitis A Outbreak

Patient no.	Age	Symptoms when coming to a hospital	HAV genome log10 copies/g	Anti-HAV IgM S/CO[a]	Total anti-HAV log10 mIU/ml
1	44	Fever, vomiting, malaise	5.27	1.82	4.37
2	57	Fever, malaise	4.60	1.90	4.90
3	50	Fever, vomiting, malaise, abdominal pain	6.41	1.99	4.86
4	56	Fever, malaise, headache	4.08	1.32	3.93
5	40	Fever, malaise, chill	2.16	1.89	4.69
6	49	Not available	2.89	1.99	5.40
7	31	Abdominal pain	3.52	2.00	5.18
8	47	Jaundice, fever, malaise, nausea	3.16	1.98	5.11
9	44	Fever, malaise, nausea	7.16	2.16	5.33
10	54	Fever, vomiting, malaise, nausea, sore-throat	5.83	2.18	5.07
11	44	Fever, malaise, nausea	1.25	1.01	2.84
12	72	Fever, malaise	6.05	2.12	4.84
13	65	Malaise, nausea, anorexia	3.86	2.33	5.18
14	61	Fever, malaise	4.61	1.80	4.34
15	47	Malaise, nausea, abdominal pain headache, diarrhea	ND[b]	0.07	ND[b]
16	15	Malaise, nausea, abdominal pain, headache	ND[b]	0.09	ND[b]
17	50	Fever, malaise, headache, chill	ND[b]	0.06	ND[b]
18	66	Fever, malaise, diarrhea, headache, chill	ND[b]	0.06	3.58
19	61	Nausea, diarrhea	ND[b]	0.05	4.10

[a]Criteria: S/CO < 0.2, negative; 0.20–1.20, equivocal, convalescence; >1.20, positive.
[b]Not detected.

detected consistently, and it was considered that both detection methods were useful for diagnosis.

The combination of anti-HAV IgM and total anti-HAV antibodies can indicate the status of individual HAV infection [Stapleton, 1995]. Serum positivity for anti-HAV IgM alone or together with total anti-HAV antibody suggests current HAV infection. On the other hand, serum positive for total anti-HAV but negative for IgM indicates historical infection. Anti-HAV IgM can be detected only during the early stage of infection, although protective anti-HAV IgG persists in the serum.

Table I shows the results of analyzing the HAV genome, anti-HAV IgM, and total anti-HAV antibody among patients exposed to the Shiga outbreak (sample group e) caused by food served in a restaurant. All individuals had dined at the restaurant when a food handler (the index case) was infected with HAV [Hasegawa et al., 2007]. Patients 1–14 were positive for anti-HAV IgM and total anti-HAV antibody and considered to be currently infected with HAV. They were admitted to a hospital for treatment immediately after diagnosis. Patients over 50 years old (the oldest being 72 years old) accounted for 50% of those with confirmed hepatitis A infection. This reflects a trend of increasing HAV-susceptibility in Japan not only among younger individuals but also among the elderly population [Kiyohara et al., 2007], despite a bias in the age distribution of diners at the restaurant.

Neither anti-HAV IgM nor the HAV genome was detectable in patients 15–19, even though all of the patients were symptomatic. Among these, patients 15–17 were also negative for total anti-HAV antibody, indicating that they had never become infected with HAV despite being susceptible. On the other hand, patients 18 and 19 were positive for total anti-HAV, and were thus protected against HAV infection. It was speculated that non-HAV pathogen(s) had caused their illness concurrently with the hepatitis A outbreak.

Hepatitis A presents with systemic symptoms such as fever, anorexia, nausea, vomiting, diarrhea, and malaise after a long incubation period (average, 28 days) [Stapleton, 1995; Fiore, 2004]. Typical hepatitis symptoms such as jaundice, dark urine, or light-colored stools might be present at the onset or follow constitutional symptoms within a few days. Infectivity peaks during the 2-week period that precedes the onset of jaundice and declines during the week after onset. In persons without jaundice, infectivity likely peaks as serum alanine aminotransferase concentrations increase [Fiore, 2004]. During the incubation period and subsequent constitutional symptoms, patients might not be aware of being infected with hepatitis A, which encourages its spread. The symptoms of all patients exposed to the Shiga outbreak were essentially the same (Table I), which caused difficulties with discriminating confirmed hepatitis A from other conditions. The principal complaints of patients with confirmed hepatitis A infection upon arrival at the hospital were not typical of hepatitis, except for one patient who had jaundice (underlined in Table I).

Fecal-oral transmission is the route of HAV infection, and personal contact is one of the most important risk factors reported [Stapleton, 1995]. Thus, patients infected with HAV should be diagnosed immediately and physicians or hospitals should report promptly to public health officials to prevent transmission and reduce the magnitude of an outbreak. Such awareness can reduce person-to-person transmission and prevent secondary infection. Prompt detection of anti-HAV IgM will also help health officials to evaluate the influence of infection and take measures to control outbreaks [Schwarz et al., 2008].

The results obtained using the in-house ELISA kit were in concordance with those of a commercial IgM detection system and with HAV genome detection. The assay is simple and requires only standard ELISA equipment. The in-house anti-HAV IgM ELISA is suitable for prompt and accurate diagnosis, as well as for epidemiological studies of HAV infection.

ACKNOWLEDGMENTS

We thank T. Miyamura for his helpful discussion and encouragement.

REFERENCES

Fiore AE. 2004. Hepatitis A transmitted by food. Clin Infect Dis 38:705–715.

Hasegawa Y, Matsumoto F, Tanaka C, Ouchi Y, Hayashi K, Wakita T. 2007. Outbreak of hepatitis A virus infection caused by food served in a restaurant. Jpn J Infect Dis 60:150–151.

Iino S. 2004. Anti HAV test. Nippon Rinsho 62:462–467 (in Japanese).

Kiyohara T, Sato T, Totsuka A, Miyamura T, Ito T, Yoneyama T. 2007. Shifting seroepidemiology of hepatitis A in Japan, 1973–2003. Microbiol Immunol 51:185–191.

Schwarz NG, Revillion M, Roque-Afonso AM, Dussaix E, Giraud M, Liberpre C, Couturier E, Delarocque-Astagneau E. 2008. A food-borne outbreak of hepatitis A virus (HAV) infection in a secondary school in Upper Normandy, France, in November 2006. Euro Surveill 13:18885. Available online: http://www.eurosurveillance.org/ViewArticle.aspx?ArticleId=18885.

Stapleton JT. 1995. Host immune response to hepatitis A virus. J Infect Dis 171:S9–S14.

Totsuka A, Moritsugu Y. 1994. Hepatitis A vaccine development in Japan. In: Nishioka K, Suzuki H, Mishiro S, Oda T, editors. Viral hepatitis and liver disease. Tokyo: Springer-Verlag. pp 509–513.

Yotsuyanagi H. 2004. Detection of HAV RNA. Nippon Rinsho 62:468–473 (in Japanese).

aptara | MIM | mim'097 | Dispatch: December 3, 2008 | CE: N/A
Journal | MSP No. | No. of pages: 8 | PE: Helen

Microbiol Immunol 2008; **00**: 1–8
doi:10.1111/j.1348-0421.2008.00097.x

ORIGINAL ARTICLE

Neutralizing antibody against severe acute respiratory syndrome (SARS)-coronavirus spike is highly effective for the protection of mice in the murine SARS model

Koji Ishii[1], Hideki Hasegawa[2], Noriyo Nagata[2], Yasushi Ami[3], Shuetsu Fukushi[4], Fumihiro Taguchi[5] and Yasuko Tsunetsugu-Yokota[6]

[4]Department of Virology I, [1]Department of Virology II, [5]Department of Virology III, [2]Department of Pathology, [3]Division of Experimental Animals Research and [6]Department of Immunology, National Institute of Infectious Diseases, Tokyo, Japan

ABSTRACT

We evaluated the efficacy of three SARS vaccine candidates in a murine SARS model utilizing low-virulence Pp and SARS- CoV coinfection. Vaccinated mice were protected from severe respiratory disease in parallel with a low virus titer in the lungs and a high neutralizing antibody titer in the plasma. Importantly, the administration of spike protein-specific neutralizing monoclonal antibody protected mice from the disease, indicating that the neutralization is sufficient for protection. Moreover, a high level of IL-6 and MCP-1 production, but not other 18 cytokines tested, on days 2 and 3 after SARS-CoV infection was closely linked to the virus replication and disease severity, suggesting the importance of these cytokines in the lung pathogenicity of SARS-CoV infection.

Key words coronavirus, *Pasteurella pneumotropica*, severe acute respiratory syndrome (SARS).

A new disease called SARS originated in China in late 2002 and spread rapidly throughout a number of countries. Structural characterization of the SARS-CoV and characterization of its complete RNA genome (1–3) have provided us with the opportunity to develop a SARS vaccine. Like other coronaviruses, SARS-CoV is a plus-stranded RNA virus with a 30-kb genome encoding replicase gene products and four structural proteins (i.e. spike [S], envelope [E], membrane [M], and nucleocapsid [N]) (1, 2). The S protein is a type I fusion protein with an approximate molecular weight of 180 kDa. The angiotensin-converting enzyme 2 (ACE2) has been reported to function as a receptor for SARS-CoV (4), and amino acids 270–510 of the S protein are required for interaction with the receptor (5), suggesting that the S protein would be an ideal target for a vaccine. In fact, passive transfer of neutralizing antibody can prevent replication of the SARS-CoV in the mouse respiratory tract (6, 7), and many vaccine studies of SARS-CoV have identified the S protein among other SARS-CoV structural proteins as a major determinant of neutralization (8).

Developing an animal model is crucial for evaluating the vaccine efficacy on SARS-CoV-induced lung pathogeneses. SARS-CoV infection occurs transiently in the mouse and the virus is cleared by day 7 postinfection (7), although an age-related susceptibility to lung disease in old mice has been shown (9). In the course of studying the cell entry mechanism of SARS-CoV, we found that some proteases, such as trypsin and elastase, produced in the host animals enhance SARS-CoV infection in cultured cells (10). In a previous study, we examined whether weak inflammation in the lungs induced by low-pathogenicity bacterial infection, which could induce elastase, enhances SARS-CoV infection and we showed that low-virulence

Correspondence
Yasuko Tsunetsugu-Yokota, Department of Immunology, National Institute of Infectious Diseases, Shinjuku-ku, Tokyo 162-8640, Japan. Tel: +81 3 5285 1111 ext. 2133; fax: +81 3 5285 1150; email: yyokota@nih.go.jp

Received 2 September 2008; revised 5 October 2008; accepted 22 October 2008

List of Abbreviations: CoV, coronavirus; IFN, interferon; Ig, immunoglobulin; IL, interleukin; IP, IFN-inducible protein; MCP, monocyte-chemotactic protein; Pp, *Pasteurella pneumotropica*; SARS, severe acute respiratory syndrome; TNF, tumor necrosis factor.

© 2008 The Societies and Blackwell Publishing Asia Pty Ltd

Pp infection, as well as administration of lipopolysaccharide derived from *Escherichia coli*, induced elastase in the lungs and enhanced the replication of SARS-CoV, which resulted in the exacerbated respiratory disease caused by SARS-CoV infection with a high mortality rate. These results indicate that coinfection of SARS-CoV with low-virulence microorganisms induces exacerbated pneumonia and suggest the possibility that elastase is involved in the pathogenesis of exacerbated pneumonia caused by SARS-CoV infection (11).

In our research group, UV-inactivated and UV- and formalin-inactivated whole virion vaccines were produced and both were shown to be effective on the elicitation of persistent neutralizing antibodies accompanied by T-cell responses (12). We also constructed a replication-deficient recombinant vaccinia virus, DIs, expressing one or more SARS-CoV structural proteins (E, M, N and S, or a combination of E, M and S (E/M/S) or E, M, N and S (E/M/N/S)) (13). When these recombinant DIs vaccines were given to mice either s.c. or intranasally, the humoral and cellular immunities against SARS-CoV were elicited. We showed that a high level of serum neutralizing IgG antibody elicited by subcutaneous injection of these vaccinias strongly suppressed SARS-CoV replication in the lungs and that the neutralizing IgA-type antibody elicited only by mucosal (intranasal) immunization was not absolutely required. Furthermore, we demonstrated that DIs expressing the S protein alone or in combination with other components, but not N alone, elicited strong neutralizing antibody and T-cell responses against SARS-CoV infection. Although we and others demonstrated that the vaccine expressing the S protein alone was able to inhibit SARS-CoV replication efficiently in mice, the role of the N-specific T-cell response for protection had not been formally excluded, because the SARS-CoV infection in mice is usually cleared rapidly without causing any pulmonary disease.

Utilizing a murine model system of severe respiratory disease caused by the coinfection of Pp and SARS-CoV, we here evaluated the protective efficacy of our SARS vaccine candidates: UV- or UV-plus-formalin-inactivated whole virion and recombinant DIs expressing the S protein only. We have monitored the bodyweight and analyzed the virus replication and cytokine production in the lung lavage of vaccinated and naïve mice after SARS-CoV infection. By giving SKOT-20 monoclonal neutralizing antibody recognizing the S protein just before Pp infection, the mortality of mice coinfected with Pp and SARS-CoV was dramatically reduced in a dose-dependent manner. These results clearly show that the neutralizing antibody against S protein is highly effective and sufficient to prevent SARS development. Furthermore, we found that IL-6 and MCP-1 production was associated with high titers of SARS-CoV, suggesting the possible link between the increased production of these cytokines and the lung pathogenicity caused by Pp and SARS-CoV coinfection.

MATERIALS AND METHODS

Virus and virus titration

Fr-mo, the mouse-adapted Frankfurt-1 (Fr-1) strain created by passaging 10 times through the mice and finally grown in VeroE6 cells, was propagated and plaque assayed with VeroE6 cells as previously described (10). VeroE6 cells were grown and maintained in Dulbecco's modified minimal essential medium (DMEM; Nissui, Tokyo, Japan) and virus infectivity was determined by plaque assay as previously described (10).

Preparation of UV- or UV-and-formalin-inactivated purified SARS-CoV

UV-inactivated purified SARS-CoV (UV-V) was prepared as previously described (14). In brief, SARS-CoV (HKU29849) was amplified in Vero E6 cells, exposed to UV light (4.75 J/cm^2), and then purified by sucrose density gradient centrifugation. A portion of the UV-inactivated purified virions was further treated overnight with 0.02% formalin (UV-F-V) to assure the safety of a whole virion vaccine (12).

Vaccination

Animal studies were carried out under a protocol approved by the Animal Care and Use Committee of the National Institute of Infectious Diseases, Japan. Six-week-old BALB/c male mice were purchased from SLC(Hamamatsu, Japan) or Charles River Japan (CRJ, Tokyo, Japan). These mice are serologically checked to be free from infections with pathogenic microorganisms, including Pp. For vaccination with recombinant DIs, mice were immunized with 10^6 plaque-forming units (p.f.u.) of rDIs-SARS-S or DIs (as a negative control) s.c. After 4 weeks, identical titers of viruses were re-administered. For vaccination with a whole inactivated virion, mice were s.c. injected into the back with 10 μg UV-V or UV-F-V with 2 mg alum, and boosted by the same procedure 7 weeks after priming. One week later, mice were anesthetized with xylazine and ketamine by intraperitoneal (i.p.) administration and intranasally inoculated with 6×10^6 colony-forming units (c.f.u.) of Pp MaM strain (11) suspended in 20 μL PBS and kept in globe box isolators in a BSL 3 laboratory in our institute during the experimental period. One day later, the mice were intranasally challenged with 0.8×10^6 $TCID_{50}$ of SARS-CoV in 20 μL saline as previously described (11). Three, 5, and 7 days after challenge by SARS-CoV, serum,

© 2008 The Societies and Blackwell Publishing Asia Pty Ltd

nasal and lung lavage fluids were collected to measure viral titers and antibodies against SARS-CoV from mice that were killed under anesthesia with chloroform. The bodyweight of these mice was measured every day.

Detection of SARS-CoV-specific antibodies

IgG titers against SARS-CoV were determined by ELISA as previously described (14). Neutralization antibody titers were determined as previously described (15). Briefly, samples were heat-inactivated and diluted twofold from 1:80 to 1:5120 with DMEM containing 5% fetal bovine serum and 3000 infectious units of vesicular stomatitis virus (VSV) pseudotype-bearing SARS-CoV S protein (VSV-SARS-St19). The mixture was incubated for 1 hr at 37 °C for neutralization. After incubation, the mixture was inoculated onto Vero E6 cells seeded on 96-well plates. The infectivity of VSV-SARS-St19 was determined by counting the number of green fluorescence protein (GFP)-positive cells. The Nab titer was defined as the reciprocal of the highest dilution at which more than 50% inhibition of infectivity was observed.

Analysis of cytokines and chemokines

Cytokines and chemokines were assayed either using a mouse inflammatory cytokine (IL-6, IL-10, MCP-1, IFN-γ, TNF-α and IL-12p70) cytometric bead array kit (Becton Dickinson, San Jose, CA, USA) (12) or using the Luminex 200 system (Luminex Co., Austin, TX, USA) as previously reported (16). Lung homogenates prepared as described above were diluted 1:10 with a lysis buffer and viruses included in the materials were completely inactivated by UV irradiation for 10 min. In the Luminex system, the following cytokines and chemokines were measured by a mouse cytokine 20 plex antibody bead kit (Bioscience International, Inc., Camarillo, CA, USA): fibroblast growth factor basic, granulocyte–macrophage colony-stimulating factor, IFN-γ, IL-10, IL-12, IL-13, IL-17, IL-1α, IL-1β, IL-2, IL-4, IL-5, IL-6, IL-10, keratinocyte-derived chemokine (KC), MCP-1, monokine-induced by IFN-γ, IFN-inducible protein (IP)-10, TNF-α, and vascular endothelial growth factor (VEGF).

RESULTS

Efficacy of a whole inactivated SARS-CoV virion vaccine and recombinant DIs expressing S protein

We studied the SARS vaccine efficacy using a recently established murine SARS model (11). In this model, a low-virulence Pp infection exacerbates lung pathogenesis associated with SARS-CoV infection.

We first examined the protective efficacy of UV- and UV-plus-formalin-inactivated whole virion (UV-V and UV-F-V, respectively). Twelve mice in each group were s.c. inoculated with 10 μg UV-V or UV-F-V with alum, or alum in PBS (alum only) as a control, booster immunized with the same vaccines at 7 weeks, and then infected with Pp intranasally 1 week later. One day after the infection of Pp, mice were intranasally infected with a mouse-adapted strain of SARS-CoV (Fr-mo). Although Pp is of low virulence and causes only a mild respiratory disease, Pp-infected mice showed a transient loss of bodyweight and ruffled hair from 1 to 3 days postinfection and then gradually recovered. However, mice coinfected with SARS-CoV 1 day after Pp infection had severe weight loss and showed high mortality with exacerbated pneumonia (11). In this murine model of SARS, both control and UV-V- or UV-F-V-vaccinated mice showed a transient decrease in bodyweight until day 2 after SARS-CoV infection (Fig. 1). Then, most of the vaccinated mice recovered to their original weight before SARS-CoV infection, whereas control mice (alum only) continuously lost weight and 90% died at day 7 postinfection.

In a second set of experiments, mice were immunized with recombinant DIs-S or empty DIs (as a negative control: DIs-cont) 5 weeks and 1 week before Pp infection, and infected with SARS-CoV the next day. Similar to the results of whole virion vaccines as described above, mice vaccinated with DIs showed transient and minimal clinical symptoms, such as ruffled hair and weight loss until 3 days after Fr-mo infection (Fig. 2, left). Severe symptoms continued during the observation period in control mice. On days 4–7 after virus infection, these mice suffered the loss of 40% or more of their bodyweight, and more than 80% of those mice died after exhibiting severe respiratory disease, whereas none of the mice vaccinated with recombinant DIs expressing S proteins died (Fig. 2, right). To further evaluate the vaccine effect, we measured serum neutralizing antibody and SARS-CoV titer in the lung lavage of vaccinated mice. Before Pp and SARS-CoV coinfection, vaccinated mice developed a high level of anti-SARS-CoV IgG with neutralizing activity (data not shown). As shown in Figure 3a, a high level of neutralizing antibody was maintained during coinfection experiments, at day 3 until day 7 postinfection in all vaccinated mouse groups. The SARS-CoV titer in the lung lavage was high at day 3 postinfection, decreased at day 5 (Fig. 3b, blank column: alum only and DIs-cont) and virus became undetectable at day 7 (data not shown). In contrast, the virus titers were significantly reduced in parallel with a high titer of plasma neutralizing antibody in all vaccinated groups (Fig. 3a). Therefore, both whole virion vaccines and vaccinia vector expressing spike protein were protective from a highly pathogenic pulmonary infection of SARS-CoV in

© 2008 The Societies and Blackwell Publishing Asia Pty Ltd

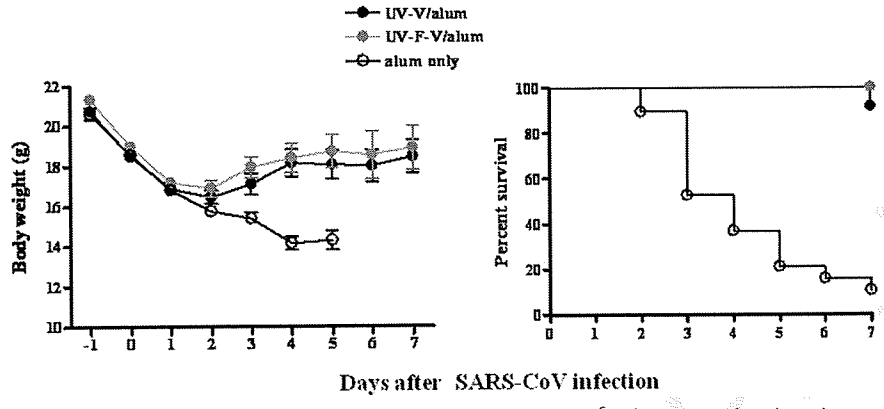

Fig. 1. (Left) Bodyweights of mice vaccinated with inactivated virions in a murine model system of severe respiratory disease caused by the coinfection of Pp and SARS-CoV. Mice were s.c. injected on the back with 10 μg UV-V or UV-F-V with 2 mg alum, and boosted by the same procedure 7 weeks after priming. One week later, mice were infected intranasally with Pp (6×10^6 c.f.u. day -1) and 1 day later with SARS-CoV (0.8×10^6 p.f.u. Fr-mo, day 0), and were weighed daily after Pp infection. Mice were vaccinated with UV-inactivated virions with alum (●), UV- and-formalin-inactivated virions with alum (◉), or alum only (○). The number of mice used in this study was 17 (UV-V), 12 (UV-F-V) and 17 (alum), respectively. Bar shows the standard error of the mean (SEM). (Right) Survival curves of mice vaccinated with inactivated virions.

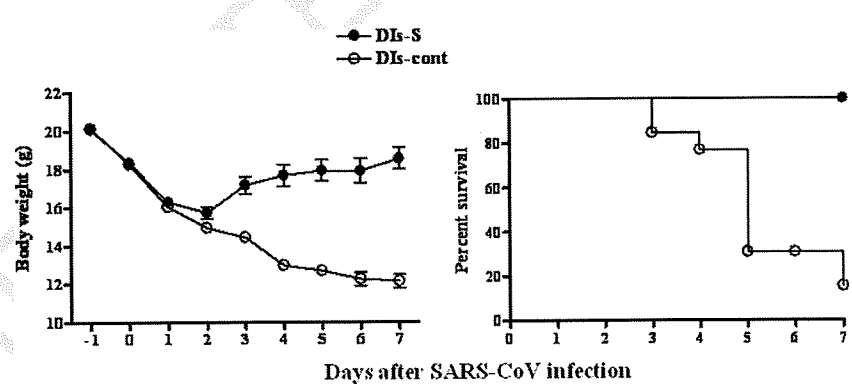

Fig. 2. (Left) Bodyweights of mice vaccinated with recombinant DIs in a murine model system of severe respiratory disease caused by the coinfection of Pp and SARS-CoV. Mice were i.p. injected with 10^6 p.f.u. of rDIs-SARS-S or DIs, and boosted by the same procedure 4 weeks after priming. One week later, mice were infected intranasally with Pp (day -1) and 1 day later with SARS-CoV (day 0), and were weighed daily after Pp infection. Mice were vaccinated with rDIs-SARS-S (●) or DIs only (○). Bar shows the SEM ($n = 18$). (Right) Survival curves of mice vaccinated with recombinant vaccinia virus.

the presence of opportunistic infection by Pp in this case. Furthermore, the results by DIs-S vaccine suggest that the neutralizing antibody against SARS-CoV spike protein alone is highly effective for the prevention of SARS development.

Inflammatory cytokines are suppressed in vaccinated mice

Ami *et al.* (11) demonstrated previously that the levels of IP-10 and IFN-γ are significantly high in SARS-CoV-infected and Pp/SARS-CoV-coinfected mouse lung homogenates at 2 days after SARS-CoV infection. However, these cytokines became undetectable at day 4 postinfection. To better understand the involvement of cytokines in the lung pathogenesis of SARS, we simultaneously measured six cytokines (IL-6, IL-10, MCP-1, IFN-γ, TNF-α and IL-12p70) in the lung lavage of vaccinated or unvaccinated mice at day 3 after SARS-CoV infection, when viruses replicate most extensively and vaccinated mice experienced maximum weight loss. As shown in Figure 4, the increased production of MCP-1 and IL-6 in the lungs of the control mouse group (alum and DIs-cont) was strongly suppressed in vaccinated mice, which were able to control virus replication. Increased production of other cytokines, including TNF-α, was not observed. Therefore, it is possible that IL-6 and MCP-1 play a role in the establishment of lung pathology in the Pp and SARS-CoV coinfection model.

Neutralizing monoclonal antibody against S protein is highly effective for protection

It is known that many of the neutralizing antibodies against SARS-CoV recognize a receptor-binding domain (RBD) in S1 of the spike protein, although other N-terminal domains of the S1 and S2 domains also have neutralizing epitopes (8). Previously, we established four S-protein-specific monoclonal antibodies with potent *in vitro* neutralization activity (17). Among them, a major

© 2008 The Societies and Blackwell Publishing Asia Pty Ltd